Optimal Design and Control of Differential Power Processing Converters for Partially Shaded Photovoltaic Array

MSc Electrical Engineering and Renewable Energy Systems

{Individual Project Report}

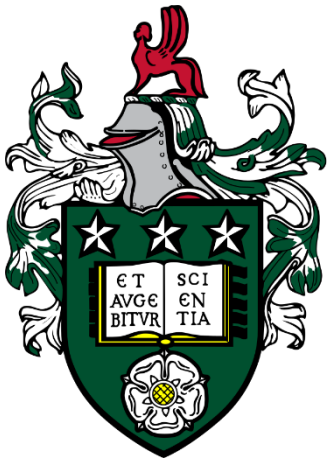

UNIVERSITY OF LEEDS

SCHOOL OF ELECTRONIC AND ELECTRICAL ENGINEERING

Abdullah Essa,
Dr. Benjamin Chong (Supervisor)
Dr. James McLaughlan (Assessor)

2022/23

ABDULLAH J. ESSA (AUTHOR), FROM KUWAIT, AN ELECTRONIC & ELECTRICAL ENGINEER, HAS A GROWING SPECIALTY IN RENEWABLE ENERGY SYSTEMS AND POWER ELECTRONICS. HOLDING A MASTER'S DEGREE FROM THE UNIVERSITY OF LEEDS, HE CONDUCTED SEMINAL RESEARCH ON THE OPTIMIZATION OF DIFFERENTIAL POWER PROCESSING (DPP) CONVERTERS FOR PHOTOVOLTAIC ARRAYS UNDER PARTIAL SHADING VIA HEURISTIC APPROACHES THROUGH WAVEFORM ANALYSIS. THIS WORK HAS THE POTENTIAL TO ENHANCE THE POWER EXTRACTION PERFORMANCE OF SOLAR INSTALLATIONS. COUPLED WITH HIS EARLIER INVESTIGATIVE WORK INTO THERMAL POWER PLANTS DYNAMIC DISPATCH CONSIDERING ROLL-OUT OF ELECTRIC VEHICLES, ABDULLAH CONSISTENTLY PROVES HIS CAPACITY TO TACKLE COMPLEX CHALLENGES IN THE ENERGY DOMAIN VIA HEURISTIC OPTIMIZATION METHODS. HIS ACADEMIC ACHIEVEMENTS ARE UNDERPINNED BY BOTH HIS DEGREES AND RESEARCH EXPERIENCE, ENSURING THAT HIS CONTRIBUTIONS TO THE ELECTRICAL ENGINEERING LANDSCAPE ARE BOTH INNOVATIVE AND APPLICABLE.

DR. BENJAMIN CHONG (SUPERVISOR), SITUATED AT THE HEART OF THE SCHOOL OF ELECTRONIC & ELECTRICAL ENGINEERING, DR. BENJAMIN CHONG IS A BEACON OF KNOWLEDGE AND EXPERTISE IN ELECTRICAL ENGINEERING, POWER ELECTRONICS, AND RENEWABLE ENERGY SYSTEMS. HAVING BEEN HONOURED AS THE BEST LECTURER MULTIPLE TIMES, HIS DEDICATION TO EDUCATION AND HIS CONTRIBUTION TO THE SEMINAL TEXTBOOK "MODERN CONTROL SYSTEMS" IS A TESTAMENT TO HIS PROWESS IN THE FIELD. DR. CHONG'S PROFESSIONAL JOURNEY BEGAN WITH A BENG IN ELECTRONIC & ELECTRICAL ENGINEERING AND LATER A PHD FROM THE UNIVERSITY OF LEEDS. HIS REAL-WORLD EXPERIENCE INCLUDES A TENURE AS AN ELECTRICAL ENGINEER AT BATANG AI HYDROELECTRIC POWER STATION IN MALAYSIA. HE PREVIOUSLY MANAGED THE MSC ELECTRICAL ENGINEERING AND RENEWABLE ENERGY SYSTEMS PROGRAM, AND CONSISTENTLY CONTRIBUTES TO INNOVATIVE RESEARCH IN AREAS LIKE GRID CONNECTION OF RENEWABLE ENERGY SYSTEMS AND ENERGY MANAGEMENT IN VARIOUS ELECTRIC SYSTEMS. AS AN EDUCATOR, HE HAS HISTORY IN LEADING THE CHARGE IN MODULES RELATED TO POWER ELECTRONICS, CONTROL, AND ELECTRIC DRIVES WHILE MENTORING THE NEXT GENERATION OF ENGINEERS THROUGH UNDERGRADUATE AND POSTGRADUATE PROJECTS.

More Info at: Dr Benjamin Chong | School of Electronic and Electrical Engineering | University of Leeds

DR JAMES MCLAUGHLAN (ASSESSOR), IS AN ASSOCIATE PROFESSOR AND AN EXPERT IN DIAGNOSTIC ULTRASOUND AND HIGH INTENSITY FOCUSED ULTRASOUND, EMBARKED ON HIS ILLUSTRIOUS CAREER WITH AN M.PHYS. FROM BATH UNIVERSITY AND VITAL RESEARCH AT THE RUTHERFORD APPLETON LABORATORIES. HIS NOTABLE PH.D. WORK AT THE INSTITUTE OF CANCER RESEARCH FOCUSED ON ULTRASOUND CANCER TREATMENTS. JOINING THE UNIVERSITY OF LEEDS IN 2010, HE PIONEERED THERAPEUTIC MICROBUBBLE TREATMENTS FOR COLORECTAL CANCER AND, BY 2013, HAD SECURED A LEVERHULME EARLY CAREER FELLOWSHIP FOR INNOVATIVE BREAST CANCER RESEARCH. AS A JOINT UNIVERSITY ACADEMIC FELLOW SINCE 2015, HE BRIDGES TECHNOLOGICAL ADVANCEMENTS IN ENGINEERING WITH DIRECT CLINICAL APPLICATIONS, WHILE ALSO CONTRIBUTING SIGNIFICANTLY TO STUDENT EDUCATION AND SERVING AS DEPUTY DIRECTOR AT IRASS.

More Info at: Dr James McLaughlan | School of Electronic and Electrical Engineering | University of Leeds

ACKNOWLEDGEMENT

THE AUTHOR WOULD LIKE TO EXPRESS MY SINCERE GRATITUDE TO ALLAH FOR HIS GUIDANCE AND BLESSINGS THAT HAVE ENABLED ME TO UNDERTAKE THIS JOURNEY. HIS HEARTFELT THANKS GO TO DR. BENJAMIN CHONG, WHOSE EXCEPTIONAL SUPERVISION AND INSIGHT WERE INVALUABLE IN GUIDING THIS PROJECT TO ITS FRUITFUL COMPLETION. HIS EXPERTISE AND ENCOURAGEMENT WERE VITAL IN NAVIGATING THE COMPLEXITIES OF THE WORK. HE ALSO WISHES TO ACKNOWLEDGE DR. JAMES MCLAUGHLAN, WHOSE INTERIM REPORT FEEDBACK, ALTHOUGH PROVIDED WITHOUT DIRECT COMMUNICATION, SIGNIFICANTLY CONTRIBUTED TO ENHANCING THIS RESEARCH. FURTHERMORE, DEEP APPRECIATION TO DR. MOHAMED ETARHOUNI FOR HIS PROFOUND WORK IN HIS PH.D. AND MASTER'S THESIS, WHICH LAID THE GROUNDWORK FOR THE INVESTIGATION PRESENTED IN THIS REPORT. ADDITIONALLY, DR. ETARHOUNI'S WILLINGNESS TO ELABORATE ON AREAS THAT WERE COMPLEX TO GRASP PROVIDED VALUABLE CLARITY AND UNDERSTANDING, ENRICHING THE DEPTH AND QUALITY OF THIS STUDY, THE AUTHOR IS GRATEFUL FOR HIS SUPPORT. SPECIAL THANKS GO TO DR. CRAIG EVANS, DIRECTOR OF STUDENT EDUCATION AND MSC INDIVIDUAL PROJECT MODULE LEADER, FOR HIS INSPIRING GUIDANCE AND STEADFAST SUPPORT THROUGHOUT THE AUTHOR'S BACHELOR'S STUDIES, WHICH SHARPENED THE ACADEMIC SKILLS FOR HIS MASTER'S ENDEAVOUR.AS SUCH, THIS RESEARCH WOULD NOT HAVE BEEN POSSIBLE WITHOUT THE GENEROUS SPONSORSHIP FROM THE AUTHOR'S HOME COUNTRY, KUWAIT, SPECIFICALLY THE KUWAIT MINISTRY OF HIGHER EDUCATION, WHO SUPPORTED MY ACADEMIC PURSUITS AND STAY IN LEEDS. LASTLY, THE AUTHOR RECOGNIZES HIS FAMILY, WHOSE UNWAVERING BELIEF IN HIS ABILITIES AND CONTINUAL LOVE AND SUPPORT HAVE BEEN THE CORNERSTONE OF ALL THE ACHIEVEMENTS. THEIR SACRIFICE AND ENCOURAGEMENT HAVE BEEN A CONSTANT SOURCE OF STRENGTH.

ABSTRACT

ABSTRACT— AMID A GLOBAL SHIFT TOWARDS RENEWABLE ENERGY, SPURRED BY GEOPOLITICAL TENSIONS AND ENVIRONMENTAL CONCERNS, PHOTOVOLTAIC (PV) SYSTEMS HAVE EMERGED AS A SIGNIFICANT CONTRIBUTOR. HOWEVER, THEY OFTEN FACE INEFFICIENCIES AND LOW CONVERSION RATES, ESPECIALLY UNDER MISMATCH CONDITIONS LIKE PARTIAL SHADING. THIS STUDY TARGETS THE OPTIMAL DESIGN AND CONTROL OF DIFFERENTIAL POWER PROCESSING (DPP) CONVERTERS IN PV CELLS, FOCUSING ON ENHANCING POWER EXTRACTION ACROSS VARIED WEATHER SCENARIOS. THE MAIN OBJECTIVES INCLUDE DEVELOPING A HEURISTIC OPTIMIZATION METHOD FOR DPP PV SYSTEMS USING MATLAB AND OPERATING AN OPTIMALLY DESIGNED SERIES PV-PV WITH INTEGRATED DPP THROUGH A SIMPLIFIED TRACK-AND-CONTROL METHOD ON SIMULINK. THE OPTIMAL DESIGN WAS IDENTIFIED VIA WAVEFORM ANALYSIS, EXAMINING FIVE CASES TO ACHIEVE THE BEST BALANCE BETWEEN RISE TIME AND RIPPLE, AND COMPARING FINDINGS TO ESTABLISHED ESTIMATION EQUATIONS. SUBSEQUENTLY, THE PV INTEGRATED DPP SYSTEM WAS AUGMENTED WITH "MATLAB FUNCTION" BLOCKS FOR SIMPLIFIED TRACKING AND CONTROL. SIMULATIONS UNDER IEC 61853 IRRADIANCE CONDITIONS COMPARED THE OPTIMAL APPROACH TO ESTIMATION EQUATIONS, REVEALING THE SUPERIORITY OF THE OPTIMAL APPROACH AND HIGHLIGHTING MAXIMUM POWER POINT (MPP) CONTROL ISSUES, DESPITE ACHIEVING THE REQUIRED DUTY RATIO FOR MPP OPERATION. THE RESEARCH MARKS AN ESSENTIAL PROGRESSION IN OPTIMIZING PV POWER EXTRACTION, ALIGNING WITH BROADER SUSTAINABILITY OBJECTIVES, AND LAYS A FOUNDATION FOR FUTURE ADVANCEMENTS IN RENEWABLE ENERGY TECHNOLOGY.

Contents

I. Introduction

The world, particularly Europe, is swiftly transitioning towards renewable energy sources, spurred by the adverse effects of fossil fuels [1]–[3] and the pressing need to alleviate their issue of energy Independence [4]. A significant catalyst for this change was the recent tensions between NATO and Russia over the invasion of Ukraine [4], [5], which disrupted the utilization of Russian fossil fuels by Europe [4]. This disruption has been particularly impactful as European countries rely on these fuels to decrease energy costs [6], [7] despite warnings; from Donald J. Trump, the 45th President of the United States at that time, of future similar kind consequences [8].

In response, European key players like Siemens and Siemens Gamesa are capitalizing on the intermittent wind resource both onshore and offshore [9]. Yet, solar photovoltaic (PV) continues to dominate, contributing 65% of the global capacity expansion [7]. A notable observation is the attraction of distributed applications, such as residential and commercial systems, which account for nearly half of the total PV growth. Moreover, PV panels offer benefits over wind turbines by eliminating issues such as noise pollution [10]. However, despite ongoing research and attempts at mitigation or improvement, PVs are infamously recognized for their low conversion rates and efficiencies which then requires that their power extraction from PV to load to be as efficient as possible to avoid further power loss [11].

With regards to enquiry on inefficient PV power extraction, it arises when two or more PV cells are connected in series and at least one cell experiences a reduction in solar irradiation compared to the others [12]–[16]. This partial shading issue can cause the cell with lower solar irradiation to overheat (hotspot) [11], [17]. To counter this, bypass diodes are commonly implemented [11], [13], [18], preventing thermal loss at the expense of completely bypassing the low solar irradiated cell [11], [12], [19], [20]. In other words, the available maximum possible power that could have been extracted is neglected (reduced power extraction).

Recently, differential Power Processing (DPP) is an approach that shares the objectives of bypass diodes but addresses these without entirely bypassing the affected PV cell or module [11], [21]. Additionally, as suggested by its name "differential", it operates based on the power difference between two PV cells or modules, unlike other power processing methods [1], [21]. This implies that instead of utilizing the full rated power through the converter as in an earlier method, Full Power Processing (FPP) approach, the power in the power converter is the difference between the two PV cells or modules [1], [21]. Hence, the DPP converter will experience a loss equivalent to a fraction of the power difference between the two PV cells or modules [1], [11], [21]. Thus, making it a reasonable candidate to address the partial shading effects while maintaining the required power extraction.

There are numerous configurations and applications of the DPP approach [1], [11]. In the context of the Series PV-PV DPP configuration, the approach is achievable via the use of bi-directional DC-DC converters [1], [22]. One notable converter device to be used for this method is the DC-DC bi-directional Ćuk converter due to its ability to achieve lower output current ripple compared to more common alternatives such as the bi-directional buck-boost converter [11], [23]–[25]. However, the bi-directional Ćuk is a 5th order device [11], owing to the number of passive elements in their circuitry [11], [26]. The higher order of the system, the more complex and difficult it is to predict and control [11].

As DPPs are used to mitigate the PV panel partial shading induced low power extraction, the specific optimal design for a wide range of weather conditions creating various partial shading scenarios will become complex. This is due to the implication of the Ćuk converter being high order. Therefore, this report will address the steps for the optimal design of the DC-DC bi-directional Ćuk converter components in the context of DPP via the development of a heuristic optimization method on MATLAB tailored for this problem. Consequently, confirming the optimal design by operating a miniature Series PV-PV DPP system via a common but less complex track-and-control method on Simulink

A. AIMS AND OBJECTIVES

PROJECT AIMS

THE PRIMARY AIM OF THIS WORK IS TO EXPLORE THE OPTIMAL DESIGN AND CONTROL OF DISTRIBUTED POWER POINT (DPP) CONVERTERS FOR PHOTOVOLTAIC (PV) CELLS UNDER MISMATCH CONDITIONS. THE FOCUS IS ON ENHANCING POWER EXTRACTION ACROSS A WIDE RANGE OF WEATHER CONDITIONS, THEREBY CONTRIBUTING TO THE ADVANCEMENT OF AN EFFICIENT AND ENVIRONMENTALLY FRIENDLY PV ENERGY SYSTEM.

PROJECT OBJECTIVES

- DEVELOPMENT OF A HEURISTIC OPTIMIZATION METHOD TAILORED TO A DPP PV SYSTEM USING MATLAB.
- OPERATING THE OPTIMALLY DESIGNED SERIES PV-PV WITH INTEGRATED DPP SYSTEM THROUGH A COMMON YET LESS COMPLEX TRACK-AND-CONTROL METHOD IMPLEMENTED ON SIMULINK.

II. PREREQUISITES

II. Prerequisites

A. PV CELL MODELLING

This section with regards to the literature review of (PV Cell Modelling) will delve into and introduce how a single PV cell is electrically modelled, henceforth the formulation of its equivalent circuit. Then, how this equivalent circuit alongside its operation characteristic equations will be utilized to define the PV cell model under various settings. Settings such as variation in solar irradiance, ambient temperature, and number of series/parallel connections. Furthermore, introducing a method that makes use of the PV cell characteristic equations to simulate a response to produce an I-V, P-V characteristic curve. Consequently, investigating the characteristic curves under a change in solar irradiance and temperature.

1. PV Cell Equivalent Circuit

There are various modelling approaches of the PV equivalent circuit, wherein the more accurate the required simulation is to be, the more complex the circuit and the characteristic equations become [27], [28]. This also further increases the compute time per iteration of the PV cell simulation [28] which would be undesirable for a multi-iteration simulation. However, various literature [11], [29]–[32] adopt a model often referred to as (single-diode model) for DPP PV system. This is due to good compromise between complexity/compute speed and accuracy of the simulation.

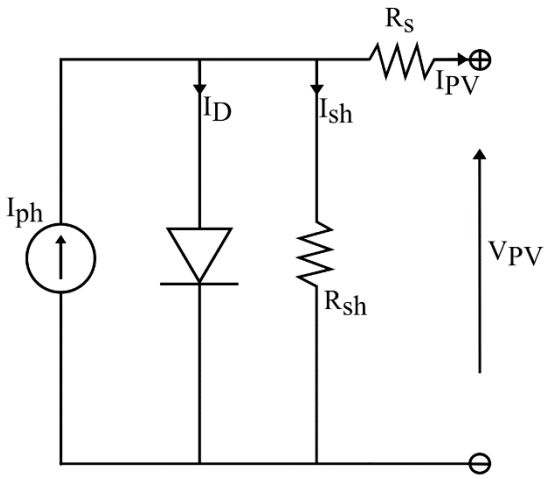

The model in **Fig. 1** incorporates the following [29], [31]–[34]:

Fig. 1: PV Cell Single Diode Model Equivalent Circuit

- **Series resistance (R_s):** Incorporated into the model to account for ohmic losses observed in junctions and terminals.
- **Shunt resistance (R_{sh}):** Represents the leakage current that finds its way to grounding when the PV cell is in reverse bias.
- **Photocurrent (I_{ph} or I_{sc}):** The current generated due to the incident light (solar irradiance) on the PV cell.
- **Diode current (I_D):** Symbolizes the dark characteristics of the PV cell, representing the current flowing through the cell when no light is present.
- **PV Output current (I_{PV}):** The current that the PV cell can provide to an external load.
- **PV cell Output Voltage (V or V_{PV}):** Signifies the voltage that the PV cell can generate under specific operating conditions.

a. PV Cell Characteristic Equations

The diode current is obtained via the following [32]–[34]:

$$I_d = I_{ph}\left(e^{\frac{qV}{AkT_c}} - 1\right) \quad (1)$$

The photocurrent is obtained via the following [32]–[34]:

$$I_{ph} = \frac{G\left(I_{ph_r} + K_i(T_c - T_r)\right)}{100} \quad (2)$$

Thus, given via KCL analysis of **Fig. 1** by:

$$I_{PV} = I_{ph} - I_d - I_{sh} \quad (3)$$

The output current ($\mathbf{I_{PV}}$) can then be written as [32]–[34]:

$$I_{PV} = I_{ph} - I_D\left(exp\left(\frac{q(V + I_{PV}R_s)}{AkT_c}\right) - 1\right) - \frac{V + I_{PV}R_s}{R_{sh}} \quad (4)$$

When considering series or parallel configurations, we substitute ($I = \frac{I}{N_P}$) and ($V = \frac{V}{N_S}$) [11], [29] which changes the equation into the following:

$$I_{PV} = n_p I_{ph} - n_p I_D\left(exp\left(\frac{q\left(\frac{V}{n_s} + \frac{I_{PV}R_s}{n_p}\right)}{AkT_c}\right) - 1\right) - \frac{\frac{Vn_p}{n_s} + I_{PV}R_s}{R_{sh}} \quad (5)$$

In the PV cell equivalent circuit model equations (1) – (5), the new variables are as follows [11], [29], [32]–[34]:

- **(G):** Solar irradiance incident to the PV cell in [$\frac{KW}{m^2}$],
- **(q):** Electron charge [$1.6x10^{-19}\ C$].
- **(A):** Diode ideality factor reflecting the characteristics of the semiconductor material used in the PV cell.
- **(k):** Boltzmann's constant, accounts for the relationship between the temperature and energy of particles. Given by [$1.38x10^{-23}m^2Kg^{-2}K^{-1}$].
- **($\mathbf{K_i}$):** Coefficient of the temperature.
- **($\mathbf{T_c}$):** PV cell temperature in Kelvin [K°].
- **($\mathbf{T_r}$):** Reference PV cell temperature in Kelvin [K°].
- **($\mathbf{I_{ph_r}}$):** The current generated due to the incident light (solar irradiance) on the PV cell at (T_R).
- **($\mathbf{n_p}$ & $\mathbf{n_s}$):** Number of PV cells connected in parallel, and number of PV cells connected in series respectively, to signify how the cells are interconnected. This influences the overall voltage and current output.

---

b. PV Cell Operational Point Compute Approach

The equation (5) is utilized to compute the consequent operational point ($\boldsymbol{I_{PV}}$). However, the equation is non-linear which requires the need of a numerical method to compute the response [11], [29]. Hence, the Newton Raphson method is utilized to estimate the operational point of ($\boldsymbol{I_{PV}}$) via root approximation given below [11], [29], [35]:

$$I_{n+1} = I_n - \frac{I_{PV}(I_n, V_n)}{I_{PV}{}'(I_n, V_n)} \quad (6)$$

$$|E| = 100\ x\left|\frac{I_{n+1} - I_n}{I_{n+1}}\right| \quad (7)$$

- **($\mathbf{V_n}$ & $\mathbf{I_n}$):** THE INPUT VOLTAGE AND OUTPUT CURRENT RESPECTIVELY OF THE PRESENT ITERATION USED TO APPROXIMATE THE NEXT (X-AXIS) POINT (I_{n+1}). THIS VOLTAGE IS ITERATED BY THE PRE-SET TOLERANCE (tol) ON EVERY ITERATION UNTIL OPEN CIRCUIT VOLTAGE (V_{OC}) IS REACHED AND RECORDED AT ($I_{PV} = 0 = I_{OC}$).
- **($\mathbf{I_{PV}}'(\mathbf{I_n}, \mathbf{V_n})$):** THE DERIVATIVE OF THE (I_{PV}) EQUATION.
- **($|\mathbf{E}|$):** THE ERROR TOLERANCE FOR THE ROOT APPROXIMATION. WHEN THIS VALUE IS EQUAL TO A PRE-SET TOLERANCE (tol), THEN THE COMPUTE PROCESS IS ENDED.

INSPIRED FROM [11], [29], [35], THE PV CELL OPERATIONAL POINT COMPUTE APPROACH IS SUMMARIZED IN THE FOLLOWING FLOWCHART.

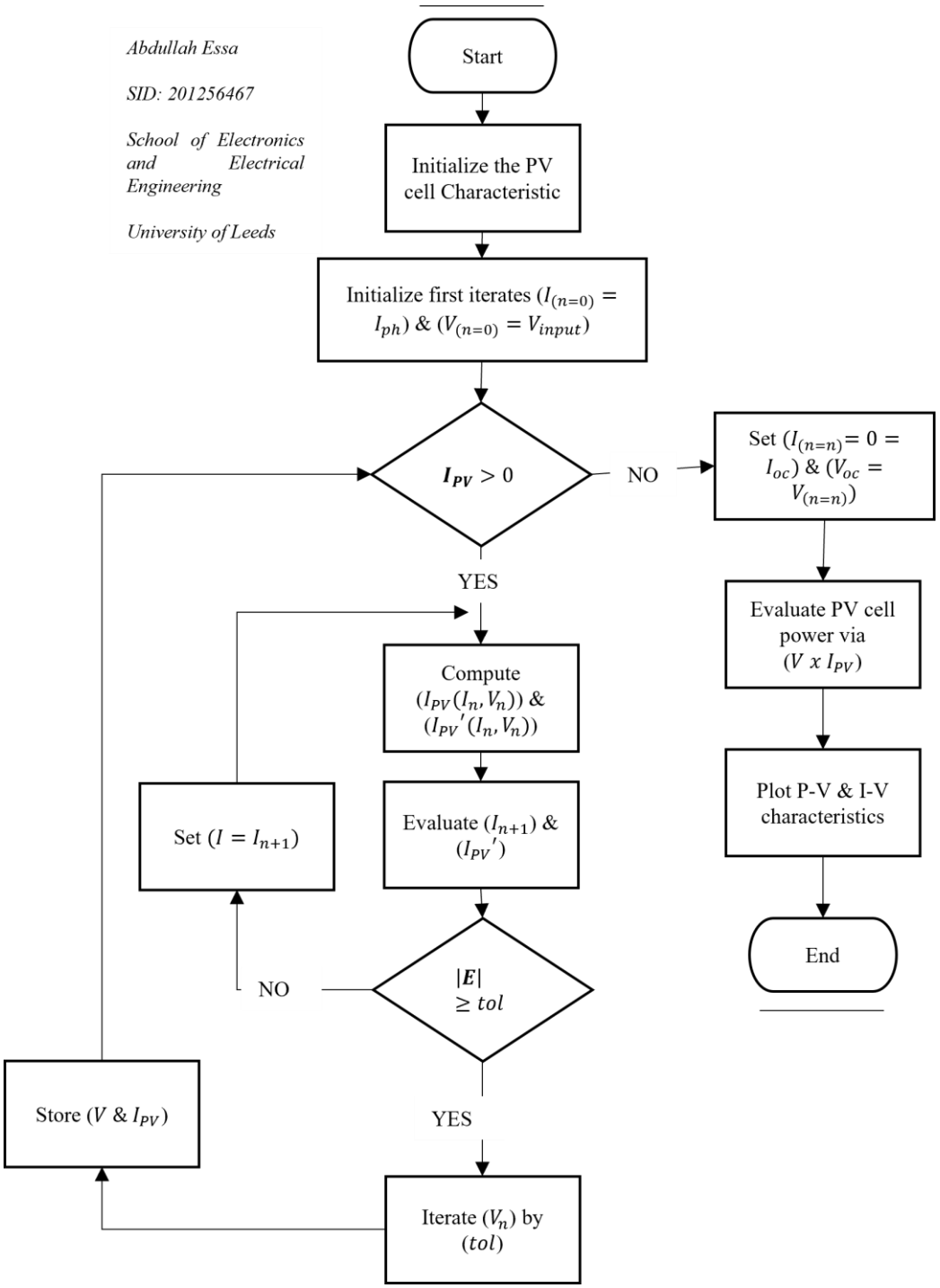

Fig. 2: PV Cell Operation Point Estimation and Plot of Characteristic on MATLAB - [Flowchart]

2. PV Cell Equivalent Circuit

In this sub-chapter, the effect of varying the PV cell temperature and solar irradiance perpendicular to the PV Panel is investigated and plotted. This is done by considering the MATLAB script in **Appendices (J)-(K)** which is defined and summarized by the flowchart in **Fig. 2**. The PV cell is initialised with PV data from [29] displayed in the following table:

Table 1: PV Characteristics Initialization Data

A	1.72
k	$1.380658x10^{-23}m^2Kg^{-2}K^{-1}$
I_d	$19.9693x10^{-6}\ A$
n_s	40
n_p	2
q	$1.6x10^{-19}\ C$
$E_g\ (Silicon\ Bandgap\ Energy\ Factor)$	1.1
K_i	$1.7x10^{-3}$
R_s	$50\ \mu\Omega$
R_p	$0.5\ M\Omega$
G	$[1000, 500, 300]\ W/m^2$
$T_a\ (Ambient\ Temperature)$	$[25, 40, 60]\ °C$
T_r	$301.18\ K$

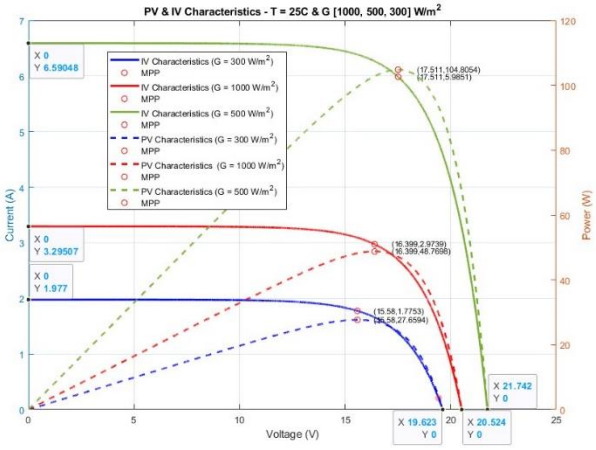

Fig. 3: PV & IV Characteristics - T = 25C & G [1000, 500, 300] W/m^2

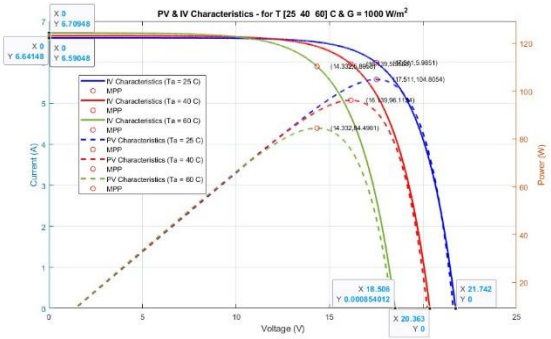

Fig. 4: PV & IV Characteristics - for T [25, 40, 60] C & G = 1000 W/m^2

Fig. 3 displays the effect of varying solar irradiation normal to the PV panel. The green response displays the I-V characteristics at test condition ($1000\ w/m^2$ & 25℃), the red response is for test condition ($500\ w/m^2$ & 25℃) and lastly, the blue response is for test condition ($300\ w/m^2$ & 25℃). The short circuit current (I_{sc}) representing the overall current being fed to the PV system from light energy [11], the maximum power point representing the operating point of the PV panel at max power [33], [36], and the open circuit voltage decrease when solar irradiation is reduced.

THE MAXIMUM POWER POINT THUS GIVEN BY THE FOLLOWING EQUATION:

$$P_{mpp} = I_{mpp}\, x\, V_{mpp} \qquad (8)$$

- **(P_{mpp}):** PV PANEL MAXIMUM OPERATING OUTPUT POWER [W].
- **(I_{mpp}):** PV PANEL MAXIMUM OPERATING OUTPUT CURRENT [A].
- **(V_{mpp}):** PV PANEL MAXIMUM OPERATING OUTPUT VOLTAGE [V].

Fig. *4* DISPLAYS THE EFFECT OF VARYING THE CELL TEMPERATURE. BLUE RESPONSE DISPLAYS THE I-V CHARACTERISTICS AT TEST CONDITION ($1000\, w/m^2$ & 25℃), THE RED RESPONSE IS FOR TEST CONDITION ($1000\, w/m^2$ & 40℃) AND LASTLY, THE BLUE RESPONSE IS FOR TEST CONDITION ($1000\, w/m^2$ & 60℃). AS TEMPERATURE INCREASES, THE CHANGE IN SHORT CIRCUIT CURRENT IS NEGLIGIBLE. HOWEVER, THE MAXIMUM POWER POINT OF THE PV PANEL, AND THE OPEN CIRCUIT VOLTAGE DECREASE. THIS IS BECAUSE WITH RISING TEMPERATURES, (I_{sc}) REMAINS RELATIVELY STABLE, WHILE (P_{mpp}) AND (V_{oc}) DECREASE. THIS TREND CAN BE ASCRIBED TO THE REDUCTION IN THE ENERGY BANDGAP OF THE SILICON CELL AT ELEVATED TEMPERATURES, WHICH LEADS TO ALTERATIONS IN THE PV PANEL'S ELECTRICAL CHARACTERISTICS [37].

3. SERIES CONNECTED PV PANEL

THE SERIES CONNECTION IS UTILIZED TO PRODUCE HIGHER VOLTAGE OUTPUTS IN PV SYSTEMS [11], [12], [32], [38] AS SHOWN IN **Fig. 5**. HOWEVER, SUCH CONFIGURATION CREATES HIGH SENSITIVITY TO DISCREPANCIES IN SOLAR IRRADIATION BETWEEN EACH CELL OR PANEL AND THE OTHER [12].

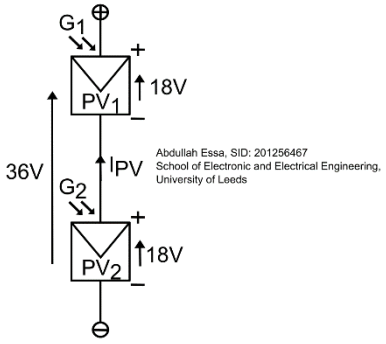

Fig. 5: Series PV Configuration

IN ESSENCE, WHEN TWO PANELS OR CELLS OF THE SAME CHARACTERISTICS ARE CONNECTED IN SERIES AND ARE EXPERIENCING EQUAL ILLUMINATION, BOTH WILL GENERATE EQUAL (I_{PH}) [11]–[13]. WHEN (I_{PH}) IS EQUAL, THE DIODES IN BOTH SYSTEMS ARE NOT IN REVERSE BIAS MODE AND THE TERMINAL TOTAL VOLTAGE IS THE SUM OF THE OUTPUT VOLTAGES OF BOTH SYSTEMS [11].

ON THE OTHER HAND, WHEN ONE OF PANELS OR CELLS (E.G., PV_1) IS EXPERIENCING LOWER ILLUMINATION, THEN (I_{PH1}<I_{PH2}). THE LARGER CURRENT (I_{PH2}) IS FORCED TO FUNNEL THROUGH (PV_1) CAUSING THE DIODE OR DIODES TO BE REVERSE BIASED. THIS MEANS (PV_1) WILL ESSENTIALLY BE CONSUMING THE POWER IT CANNOT PASS THROUGH WHICH INCREASES THE CELL TEMPERATURE CAUSING HOTSPOTS THAT DAMAGE THE CHARACTERISTICS OF THE PV CELL [19], [20], [39].

a. BYPASS DIODE APPROACH

STANDARD PRACTICE INCORPORATES BYPASS DIODES IN PARALLEL WITH PV CELL STRINGS TO AVERT HOT SPOTTING [13], [18]. WHEN FORWARD-BIASED, THESE DIODES CREATE AN ALTERNATE CURRENT PATH, PREVENTING EXCESSIVE REVERSE VOLTAGE BIAS ACROSS THE SERIES CONNECTED PV TERMINALS [40], [41]. FURTHERMORE, RESEARCH [41] SHOWS THAT BYPASS DIODES, WHEN PLACED ACROSS INDIVIDUAL PV CELLS, CONTRIBUTE TO AN INCREASE IN TOTAL DIODE VOLTAGE-DROP AS THE NUMBER OF SERIES-CONNECTED PV CELLS AND SHADED AREA

EXPANDS. INCORPORATING THAT WITH HOW BYPASS DIODES IGNORE INCOMING ENERGY FROM LOWER ILLUMINATED CELLS. THIS CREATES TWO POWER PEAKS IN THE SYSTEM, ONE REPRESENTING THE UNSHADED CELL (GLOBAL PEAK) AND THE OTHER REPRESENTING THE SHADED CELL (LOCAL PEAK). HENCE, LEADING TO A NOTABLE DECREASE IN OUTPUT POWER. THIS PHENOMENON IS SUMMARIZED IN THE FOLLOWING FIGURES TAKEN FROM [41].

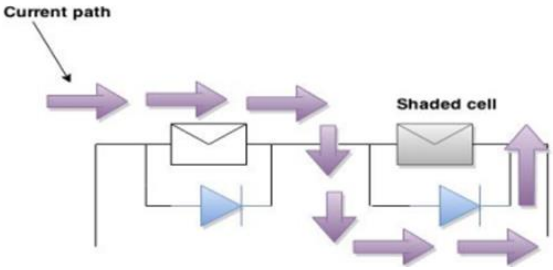

Fig. 6: Current Flow in Series Connected PV Cells Under Partial Shading with Bypass diodes

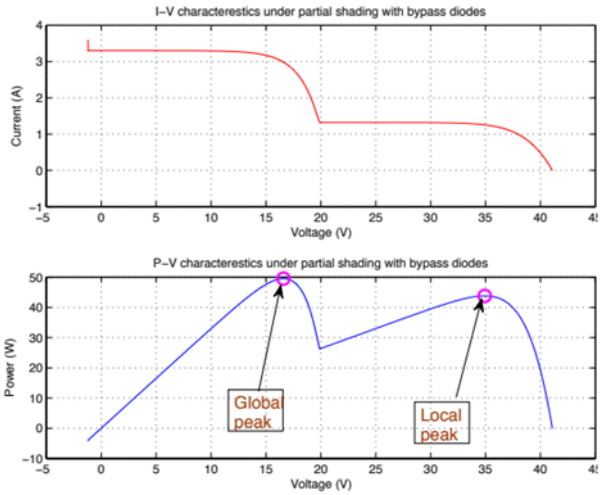

Fig. 7: I-V & P-V Characteristics Plots of Two PV Cells Connected in Series Experiencing Partial Shading with Bypass Diodes

B. DIFFERENTIAL POWER PROCESSING CONFIGURATION AND OPERATION IN PV SYSTEMS

THIS SECTION DELVES INTO THE FUNDAMENTAL CONCEPT AND STRUCTURE OF A DPP SYSTEM, WITH A SPECIFIC EMPHASIS ON ITS IMPLEMENTATION VIA A BI-DIRECTIONAL DC-DC CONVERTER.

1. SELECTION AND APPLICATION OF SERIES DPP CONFIGURATIONS IN PV SYSTEMS

THERE ARE TWO DPP STRUCTURES, SERIES AND PARALLEL [1], [11]. CONSEQUENTLY, THE STRUCTURE OF THE DPP THAT WILL BE LOOKED AT IS THE SERIES CONFIGURATION. THIS IS BECAUSE, THE CHOICE OF A SERIES CONFIGURATION, OVER PARALLEL ARRANGEMENTS, IS DETERMINED BY THE VOLTAGE REQUIREMENTS OF THE APPLICATION [1]. WHILE PARALLEL CONFIGURATIONS ARE WELL-SUITED FOR APPLICATIONS WITH VOLTAGE DEMANDS PROXIMATE TO THE PV ELEMENT'S OUTPUT, SERIES CONFIGURATIONS EXCEL IN SCENARIOS WHERE VOLTAGE REQUIREMENTS SIGNIFICANTLY DIFFER FROM THE PV ELEMENT'S OUTPUT [1]. HENCE, THE CURRENT DIFFERENCE BETWEEN ADJACENT MODULES IS UTILIZED TO GENERATE AN OUTPUT VOLTAGE THAT EXCEEDS THE PHOTOVOLTAIC ELEMENT'S ORIGINAL OUTPUT VOLTAGE [1], [41].

THE FOLLOWING **TABLE 2** SUMMARIZES THE SERIES DPP CONFIGURATIONS WITH THEIR ADVANTAGES AND DISADVANTAGES TAKEN FROM [1].

Table 2: Series DPP Configurations

Configuration	Advantages	Disadvantages
PV-bus	Reduced amount of proportional power loss.	Scalability and high coupling of return current to string current.
PV-IP	Power of each PV element can be exchanged with the independent bus directly even if the PV element has a lower voltage, lower ratings and cost.	Exact MPPT may not be achievable at any given string current due to power balance equality constraint.
PV-PV	Less DPP converters and their rating is independent of main voltage bus.	Current rating of the DPP converters increase with the PV string length.

a. SERIES PV-PV DPP CONFIGURATION

IN THE PV-PV DPP CONFIGURATION, THE MINIMIZED QUANTITY OF DPP CONVERTERS AND THEIR INDEPENDENCE FROM THE MAIN VOLTAGE BUS BECOME NOTEWORTHY. ILLUSTRATED IN **Fig. 8.A** & **Fig. 9**, FROM [1], [12], [22] THERE EXIST (N-1) DPP CONVERTERS FOR A SPECIFIED NUMBER (N) OF PV ELEMENTS. WHEN CONNECTING TWO PV MODULES WITH DIFFERING OUTPUT VALUES, THE DPP CONVERTER REGULATES THE CURRENT DIFFERENCE, DENOTED BY $(I_{PV1} - I_{PV2})$, BETWEEN THE MISMATCHED PV1 AND PV2. THIS DIFFERENTIAL CURRENT IS TRANSIENTLY CONTAINED WITHIN THE CONVERTER'S PASSIVE ELEMENTS, FOLLOWED BY A SUBSEQUENT DELIVERY TO THE OUTPUT [11], [12], [41]. THIS STRATEGY EQUALIZES THE PV MODULE VOLTAGES, ENABLING OPERATION AT THEIR INDIVIDUAL MPP PV CURRENT OUTPUTS, AS DEPICTED IN **Fig. 8.B**, CONSEQUENTLY REDUCING THE COMPONENT COUNT FOR (N) PV ELEMENTS [12].

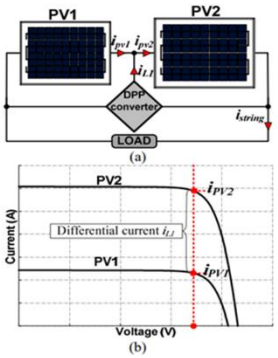

Fig. 8: (a) Series PV-PV DPP structure (b) I-V characteristics plot

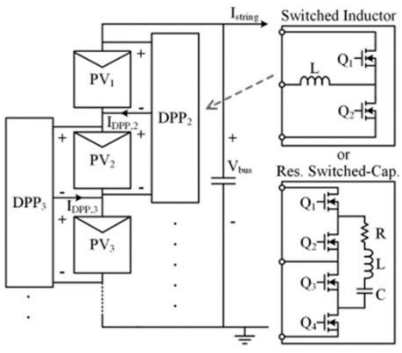

Fig. 9: Series PV-PV DPP structure switched inductor or resonant switched-capacitor from [1]

2. Choice of Converter for Differential Power Processing

As indicated in **Fig. 9**, the DPP can be realized as a bi-directional DC-DC converter with a switch-mode RLC circuit. While the Buck-Boost Converter is traditionally used for such applications such as in [21], evidence from [11], [23]–[25] suggests that the Ćuk circuit may offer superior performance, with smaller output voltage and load current ripples.

---

a. Series PV-PV DPP Configuration

Inspired from [11], [41], a miniature PV system consisting of two PV panels with a single integrated DPP converter is considered. The DPP converter will be a bi-directional Ćuk converter and the consequent circuit model is shown below in **Fig. 10**.

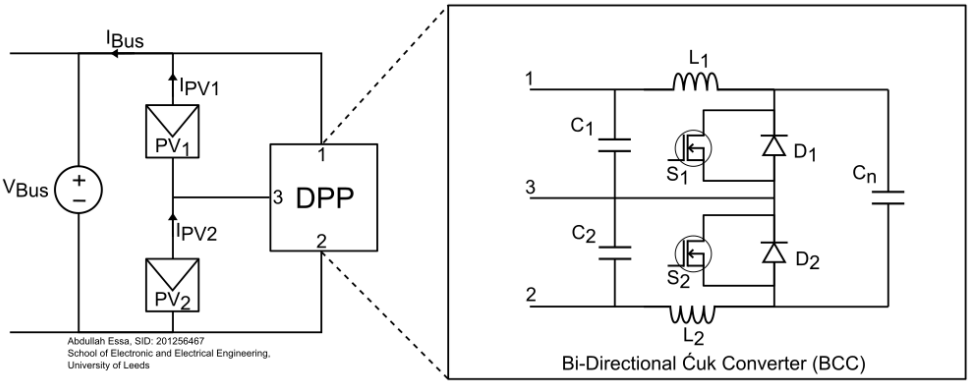

Fig. 10: PV System with Integrated Bi-directional Ćuk Converter Circuit

In the illustrated configuration, the Ćuk converter is structured with two sets of switching components: S1-D2 and S2-D1 [11]. Additionally, the Ćuk converter incorporates a capacitor, Cn, situated between the switching pairs. This capacitor is integral to the converter's operation, enabling energy transfer between terminals [11]. It's worth noting that this energy transfer isn't limited to a single direction; it can be bidirectional, which is particularly useful when solar irradiation levels vary across different PV modules [1]. Consequently, the positive input and negative output of this converter is connected in parallel to the constant DC voltage bus line shown in **Fig. 10** as (V_{Bus}) [1], [21].

With aid of measuring and tracking instruments, this system can be used to keep the PV system operating at its maximum power point even if partially shaded via the following formulation from [11], [26], [41]–[43]:

$$\left|\frac{V_{PV2}}{V_{PV1}}\right| = \frac{1-K}{K} \tag{9}$$

Such that,

$$\left|\frac{V_{PV2_{mpp}}}{V_{PV1_{mpp}}}\right| = \frac{1-K_{mpp}}{K_{mpp}} \tag{10}$$

In the PV system operating through various weather conditions, it would require that the DPP device be responsive in terms of how fast it would be able to change its operating point. This would be the operating points of voltages across (PV_1 & PV_2) and the output current (I_{Bus}) flowing towards the (V_{Bus}) line given by **equation (11)** from [41]. Additionally, low steady state ripples such that the maximum power operating points can be deduced, and external circuitry connected to the bus line are not damaged.

$$I_T = I_{PV1} + I_{L2} = I_{PV1} - I_{L1} \tag{11}$$

HOWEVER, BY MODELLING THE ENTIRE PV WITH INTEGRATED BI-DIRECTIONAL CONVERTER ĆUK SYSTEM DEDUCED FROM [11], [41], [42]. WE GET THE FOLLOWING STATE SPACE MODEL SUMMARIZING THE CHARACTERISTIC OF THE SYSTEM DURING ON AND OFF TIME:

$$\begin{bmatrix} \frac{di_{L1}}{dt} \\ \frac{di_{L2}}{dt} \\ \frac{dV_{PV1}}{dt} \\ \frac{dV_{PV2}}{dt} \\ \frac{dV_{CN}}{dt} \end{bmatrix} = \begin{bmatrix} 0 & 0 & \frac{1}{L_1} & 0 & \frac{1-K_{on}}{L_1} \\ 0 & 0 & 0 & -\frac{1}{L_2} & \frac{K_{on}}{L_2} \\ -\frac{1}{C_1} & 0 & 0 & 0 & 0 \\ 0 & \frac{1}{C_2} & 0 & 0 & 0 \\ \frac{1-K_{on}}{C_N} & -\frac{K_{on}}{C_N} & 0 & 0 & 0 \end{bmatrix} \begin{bmatrix} i_{L1} \\ i_{L2} \\ V_{PV1} \\ V_{PV2} \\ V_{CN} \end{bmatrix} + \begin{bmatrix} 0 \\ 0 \\ -\frac{1}{C_1} \\ -\frac{1}{C_2} \\ 0 \end{bmatrix} i_{Bus} + \begin{bmatrix} 0 \\ 0 \\ \frac{1}{C_1} \\ 0 \\ 0 \end{bmatrix} i_{PV1} + \begin{bmatrix} 0 \\ 0 \\ 0 \\ \frac{1}{C_2} \\ 0 \end{bmatrix} i_{PV2} \quad (12)$$

- (K_{on})**:** REPRESENTS THE ON-TIME OPERATION.
- $(1 - K_{on})$**:** REPRESENTS THE OFF-TIME OPERATION.

FROM **EQUATION (12)** THE STATE SPACE MODEL WHICH IS USED TO FORMULATE THE SYSTEM TRANSFER FUNCTION [11], [42]; SHOWS THAT THE SYSTEM IS OF 5TH ORDER. THUS, COMPLEX TO ACCURATELY FIND THE SWEET SPOT FOR AN OPTIMAL RISE TIME AND LOW STEADY STATE RIPPLE AT THE SAME TIME. ADDITIONALLY, THE GIVEN EQUATIONS IN LITERATURE [11], [41] FOR THIS MODEL, EQUATIONS BELOW, CAN ONLY ESTIMATE THE COMPONENT VALUES AND AS SUCH THE RESPONSE MIGHT NOT FALL ON THE REQUIRED EXACT OPERATIONAL SWEET SPOT.

$$L_1 \geq V_{mpp1} \frac{K}{f \Delta i_1} \quad (13)$$

$$L_2 \geq V_{mpp2} \frac{1-K}{f \Delta i_2} \quad (14)$$

$$C_1 = \frac{\Delta i_1}{8 f \Delta v_1} \quad (15)$$

$$C_2 = \frac{\Delta i_2}{8 f \Delta v_2} \quad (16)$$

$$C_n \geq \left(\frac{V_{Bus} + K}{R f \Delta V_{Cn}} \right) \quad (17)$$

FOR EQUATIONS (13) – (17), THE NEW VARIABLES ARE AS FOLLOWS [41]:

- (Δi_1)**:** I_{L1} CURRENT RIPPLE GIVEN BY (I_{L1} X $\%_{RIPPLE}$)**.**
- (Δi_2)**:** I_{L2} CURRENT RIPPLE GIVEN BY (I_{L2} X $\%_{RIPPLE}$)**.**
- **(f):** SWITCHING FREQUENCY OF CHOPPING TIME OF CONVERTER.
- (Δv_1)**:** V_{PV1} VOLTAGE RIPPLE GIVEN BY (V_{PV1} X $\%_{RIPPLE}$).
- (Δv_2)**:** V_{PV2} VOLTAGE RIPPLE GIVEN BY (V_{PV2} X $\%_{RIPPLE}$).
- (ΔV_{Cn})**:** V_{CN} VOLTAGE RIPPLE GIVEN BY (V_{CN} X $\%_{RIPPLE} = V_{BUS}$ X $\%_{RIPPLE}$).
- (V_{Bus})**:** BUS LINE VOLTAGE GIVEN BY ($V_{PV1} + V_{PV2}$).

C. DIFFERENTIAL POWER PROCESSING IMPLEMENTATION AND SIMULATION

1. SERIES DPP BCC CONVERTER MODEL BUILD VIA SIMULINK

IN THIS SECTION, THE PV SYSTEM WITH AN INTEGRATED BI-DIRECTIONAL ĆUK CONVERTER CIRCUIT AS SHOWN IN **Fig. 10** IS BUILT ON THE SIMULINK SIMULATION PROGRAM. THIS SIMULINK BUILT MODEL WILL THEN BE USED TO SIMULATE THE RESPONSE OF THE SYSTEM IF IT WAS MODELLED USING THE ESTIMATION EQUATIONS (13) – (17). HENCE, THEN THE RESULTS WILL BE ANALYSED.

a. BUILD OF PV-PV DPP EMPLOYED VIA BCC ON SIMULINK

THE SIMULINK MODEL IN **Fig. 11** INCLUDES CURRENT AND VOLTAGE MEASUREMENT BLOCKS PLACED IN LOCATIONS WHERE VALUE OF OPERATIONAL POINT IS NECESSARY. ADDITIONALLY, THE FOLLOWING BLOCKS ARE USED AS WELL:

- (**PULSE_GENERATOR**): GENERATES A SQUARE WAVE SIGNAL WITH VARIABLE DUTY RATIO OF ON/OFF TIME.
- (**NOT_GATE**): USED FOR MULTIPLYING THE SQUARE WAVE SIGNAL BY (-1) FOR INVERSION TO ALLOW THE COMPLEMENTARY SWITCHING OF THE CONVERTER.
- (**OUT.X**): THIS IS USED TO EXTRACT OPERATION POINT X VALUE TO THE MATLAB SCRIPT WORKSPACE TO BE ANALYSED.

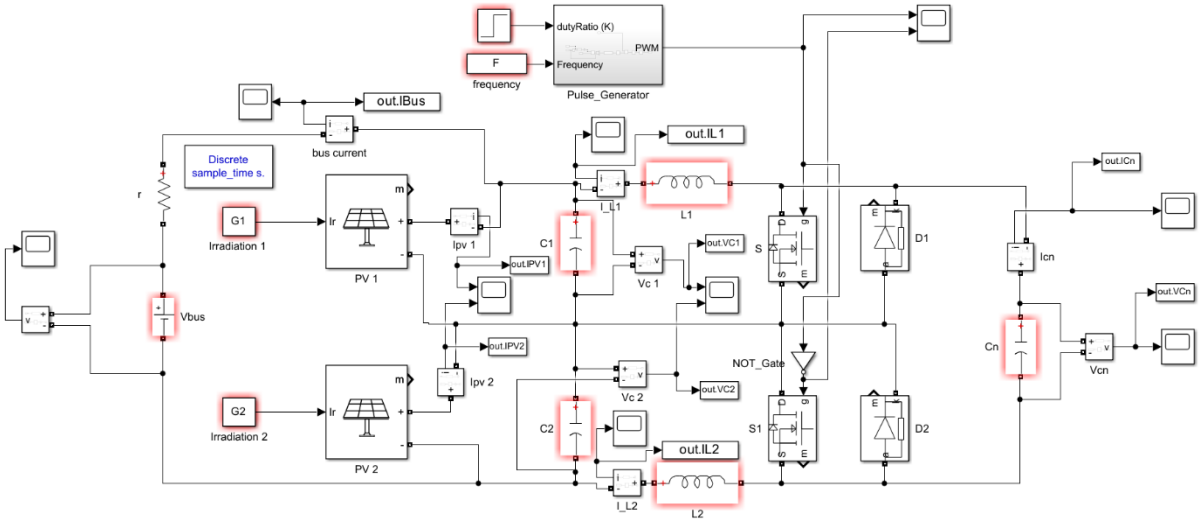

Fig. 11: PV-PV DPP employed via Integrated Bi-directional Ćuk Converter on Simulink

THE MODEL FILE IS FOUND IN **APPENDIX (H)**.

b. SYSTEM PARAMETERS

Table 3: Simulation Model Discrete Time Settings

Final Time	0.04s
Step Time	0.02s
Sample Time	$1x10^{-6}$s

THE SIMULINK MODEL IN **Fig. 11** WILL BE SIMULATED VIA THE TIME SETTINGS STATED IN **Table 3**. THIS IS TO DECREASE THE TIME REQUIRED FOR THE ENTIRE SIMULATION TO PROCESS WITHOUT CORRUPTING THE PRECISION OF

THE RESPONSE AS LONG AS $(Sample\,Time \ll f)$. ADDITIONALLY, THE TEST WILL BE CONDUCTED UPON THE SCENARIO OF PV_2 PARTIALLY SHADED $(G_{PV1} > G_{PV2})$ INITIALLY IN THE FORM OF DUTY RATIO (K = 0.45) THEN $(G_{PV1} = G_{PV2})$ IN THE FORM OF DUTY RATIO (K = 0.5).

CONSEQUENTLY, IN **Table 4**, THE CS5C-90M PV PANEL WITH ITS CHARACTERISTICS STORED WITHIN THE SIMULINK PV ARRAY BLOCK DATABASE IS UTILIZED. CONSIDERING ITS MAXIMUM POWER POINT VALUES, EQUATIONS (13) – (17), SOLAR IRRADIANCE OF $1000\,W/m^2$ AND A SWITCHING FREQUENCY OF 20 KHZ, THE PASSIVE ELEMENTS FOR THE DPP SYSTEM ARE ESTIMATED.

Table 4: Design Specifications for DPP-PV system considering CS5C-90M PV Panel Data in Simulink

PARAMETERS	SYMBOLS	VALUES
PV open-circuit voltage	V_{OC}	22.2 V
PV short-circuit current	I_{SC}	5.4 A
Irradiation	G	$1000\,W/m^2$
PV voltage MPP	V_{mpp}	18 V
PV current MPP	I_{mpp}	4.99 A
Switching frequency	f	20 kHz
Inductance at ports 1 and 2	$L_1 = L_2$	4.9 mH
Capacitance at ports 1 and 2	$C_1 = C_2$	1.59 μF
Capacitance parallel to bus line	C_n	1.59/2 μF
Bus voltage	$V_{bus} = V_{mpp}(total)$	36 V

c. SYSTEM PARAMETERS

THE SIMULATION IS RUN THROUGH THE SCRIPT FOUND IN **APPENDIX (F)** WHICH INITIALIZES MODEL, CALLS FOR ITS OPERATION, AND THEN EXTRACTS THE MEASUREMENTS DATA FROM THE (**OUT.X**) BLOCKS TO THE MATLAB SCRIPT WORKSPACE TO THEN BE ANALYZED AND PLOTTED.

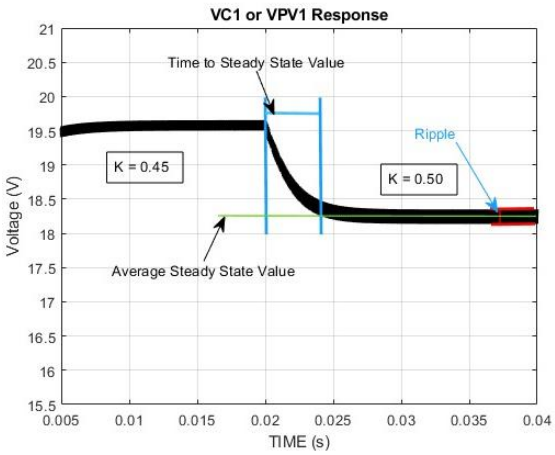

Fig. 12: Series PV System with Integrated Ćuk based DPP Converter V_{PV1} Response Plot

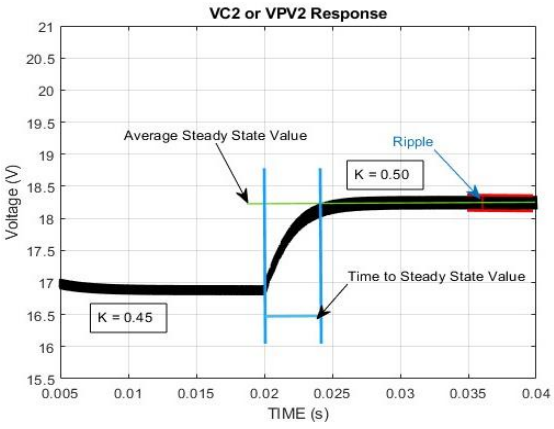

Fig. 13: Series PV System with Integrated Ćuk based DPP Converter V_{PV2} Response Plot

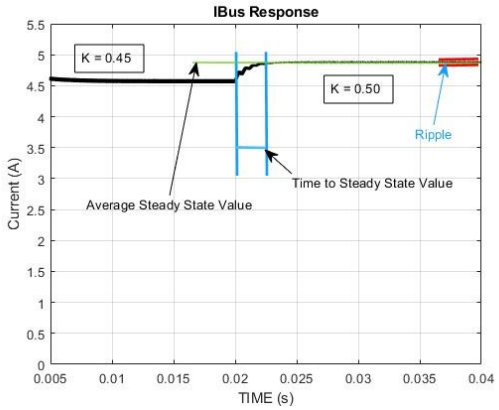

Fig. 14: Series PV System with Integrated Ćuk based DPP Converter I_Bus Response Plot

Table 5: Table of Results from the Simulink Model Simulation

Measurement	Average Steady State Value at K = 0.5	%Ripple	Time to Steady State Value
V_{PV1}	18.24 V	1.03%	44 ms
V_{PV2}	18.24 V	1.03%	44 ms
I_{Bus}	4.88 A	3.00%	31 ms

TYPICALLY, IN SWITCHING CIRCUITS WHERE DC-DC CONVERTERS ARE INVOLVED, AN OUTPUT RIPPLE OF AROUND 2% IS PREFERABLE [44]. THE ESTIMATION EQUATIONS (13) – (17) GAVE A RESPONSE THAT FITS THE PROFILE. BOTH V_{PV1} & V_{PV2} HAVE A RIPPLE OF 1.03% AND THE I_{Bus} HAS A RIPPLE OF 3%.

ADDITIONALLY, THE VOLTAGE LEVELS OF EACH PV PANEL ARE HOVERING AROUND THEIR THEORETICAL MAXIMUM POWER POINT AT (18.24 V) FOR DUTY RATIO OF 0.5. THE BUS CURRENT IS MAINTAINED AS CLOSE AS POSSIBLE TO ITS THEORETICAL MAXIMUM POWER POINT VALUE AT (4.88 A). THIS SHOWS THAT THE SYSTEM IS OPERATING AS INTENDED.

HOWEVER, THERE IS ROOM FOR IMPROVEMENT FOR THE TIME TAKEN TO REACH STEADY STATE AS IT IS AN OVERDAMPED RESPONSE FOR ALL THREE OF THE RESPONSES WITH 44 MS AND 31 MS FOR (V_{PV1} & V_{PV2}) AND (I_{Bus}) RESPECTIVELY. THE ESTIMATION EQUATIONS ALONE ARE NOT ENOUGH TO ACCURATELY FIND AN OPTIMAL COMPROMISE BETWEEN THE RIPPLE AND THE TIME TO STEADY STATE. CONSEQUENTLY, AN OPTIMIZATION METHOD WILL BE REQUIRED TO FIND THE OPTIMAL COMBINATION OF THE (L_1, L_2, C_1, C_2 & C_n) VALUES SUCH THAT A FASTER RESPONSE OR A CRITICALLY DAMPED SYSTEM IS ACHIEVED WHILE MAINTAINING MINIMAL RIPPLE. ADDITIONALLY, MAINTAINING MINIMAL RIPPLE ALLOWS FOR EASE OF V_{mpp} TRACKING.

THE METHOD USED TO APPROXIMATE THE RIPPLE AND TIME TO STEADY STATE VALUE IS FOUND IN **APPENDIX (E)**.

III. OPTIMIZING THE DPP SYSTEM

III. Optimizing the DPP System

In this chapter, a suitable optimization method will be selected for the improvement of the Series PV System with Integrated Ćuk based DPP Converter. This is to keep the input PV voltage and output bus current ripples at minimum whilst achieving a faster response in terms of time to reach steady state value after a step change in the duty ratio.

A. Optimization Method

Existing literature provides a detailed examination of integrated DPP converter design for PV systems, often contrasting this solution with other methods of mitigating the effects of partial shading [11], [14], [18], [31], [38], [41]. Some studies further delve into the optimization of the Ćuk converter for DPP applications, leveraging optimization techniques such as the least squares method [11], [42].

However, the literature appears to lack exploration of an optimization method specifically tailored to a 5th order PV system with an integrated Ćuk DPP, based on the particle swarm optimization (PSO) algorithm. Such an investigation could potentially yield insights on the improvements in the performance of the response for of the DPP converter in **Fig. 11**.

1. Series DPP BCC Converter Model Build Via Simulink

PSO is a computational method renowned for identifying global minima [45]–[47]. It starts by setting up particles, defining their population, and determining the iteration parameters. Throughout iterations, the algorithm tracks the personal best value for each particle and records a global best across the entire population. This mechanism equips the particles to proficiently explore the search space, as they are guided by the locations yielding better values. The exploration process adheres to **equations (18) - (19)** [45]–[47]:

$$v_{id} = w{v_{id}}^{k} + C_1\left(P_{best_{id}} - {x_{id}}^{k}\right) + C_2(G_{best_d} - {x_{id}}^{k}) \quad (18)$$

$$x_{id}^{(k+1)} = {x_{id}}^{k} + {v_{id}}^{(k+1)} \quad (19)$$
$$i = 1, 2, \dots, N_p$$
$$d = 1, 2, \dots, N_g$$

- **(N_g):** Represents the number of dimensions.
- **(N_p):** Represents the particle population size.
- **($P_{best_{id}}$):** Represents the best position so far for particle (i) at dimension (d).
- **(G_{best_d}):** Represents the best position among all particles through (i) dimensions.
- **(v_{id}):** Represents the velocity of particle (i) at dimension (d).
- **(x_{id}):** Represents the position of particle (i) at dimension (d), the position is used to compute the fitness to identify single dimension value of the multidimensional particle.
- **(C_1 & C_2):** Provide weighting of the deviation from a particle's best self-performance.
- **(w):** Represents the inertia of a particle.

2. Series DPP BCC Converter Model Build Via Simulink

For the PSO algorithm to work, it would need a way to analyse the responses of (V_{PV1}, V_{PV2} & I_{Bus}). This analysis would need to allow the algorithm to basically give a value to the whole response type reflecting the ripple size and the time to steady state value. Essentially allowing the identification of a possible minimum ripple and time to steady state value.

a. TAILORED FITNESS FUNCTION

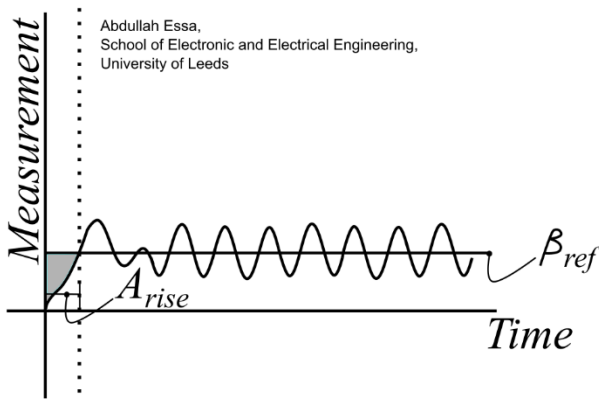

Fig. 15: Example Showcase of Time to Steady State and/or Rise Time Area

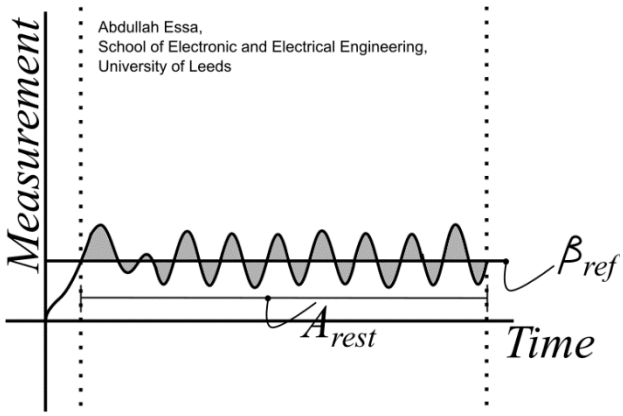

Fig. 16: Example Showcase of Ripple Area

THE VALUE REFLECTING THE RIPPLE AND TIME TO STEADY STATE VALUE IS NAMED THE FITNESS. THIS FITNESS IS FOUND BY FIRST EXTRACTING THE SIGNAL RESPONSE THROUGH THE (**OUT.X**) BLOCK TO THE MATLAB SCRIPT WORKSPACE, DEDUCING THE AVERAGE STEADY STATE VALUE, AND THEN FIND THE ABSOLUTE AREA ABOVE AND BELOW THIS STEADY STATE VALUE LINE AS SUMMARIZED IN **Fig. 15** AND **Fig. 16**.

FINDING THE AVERAGE STEADY STATE VALUE IS GIVEN BY,

$$\beta_{ref} = \left(\frac{1}{round(0.1n)}\right) \sum_{x=n-round(0.1n)}^{n} [\beta_x] \quad (20)$$

THE AREA VALUE FOR RESPONSE THROUGH TIME UNTIL STEADY STATE VALUE IS REACHED,

$$A_{rise} = \left|\beta_{rise} - \beta_{ref}\right| \quad (21)$$

THE AREA VALUE FOR RESPONSE THROUGH STEADY STATE TO FIND THE FITNESS OF THE RIPPLE,

$$A_{rest} = \left|\beta_{rest} - \beta_{ref}\right| \quad (22)$$

THE TOTAL FITNESS FOR THE RESPONSE IS THEN GIVEN BY,

$$FF = \frac{(w_1 \sum A_{rise} + w_2 \sum A_{rest})}{simulation\ time} \quad (23)$$

- **(n):** REPRESENTS THE NUMBER OF DISCRETE DATA POINTS IN THE WAVEFORM.
- **(β_x):** REPRESENTS THE DISCRETE VALUE OF A DATA POINT IN THE WAVEFORM AT LOCATION (x).
- **(β_{ref}):** REPRESENTS THE AVERAGE COMPUTED AREA OF THE LAST 10% OF THE WAVEFORM SERVING AS THE REFERENCE.
- **(A_{rise}):** THE AREA OUTSIDE THE REFERENCE LINE THROUGH RANGE OF VALUES UNTIL THE REFERENCE LINE IS MET.
- **(A_{rest}):** AFTER THE REFERENCE LINE IS MET, THE REST OF THE AREA OUTSIDE THE REFERENCE LINE IS COMPUTED.
- **(w_1):** REPRESENTS THE PRIORITY WEIGHT GIVEN TO THE NORMALIZED AREA FITNESS OF TIME UNTIL STEADY STATE VALUE.
- **(w_2):** REPRESENTS THE PRIORITY WEIGHT GIVEN TO THE NORMALIZED AREA FITNESS OF STEADY STATE REGION.
- **(FF):** REPRESENTS THE FITNESS VALUE OF THE RESPONSE WAVEFORM DIVIDED BY TOTAL SIMULATION TIME TO NORMALIZE.

---

b. OPTIMIZATION ALGORITHM "FLOWCHART"

IN THIS SECTION, FLOWCHARTS OF FITNESS VALUE ATTAINMENT METHOD FOR THE PV VOLTAGE RESPONSE AND BUS CURRENT RESPONSE ARE FORMULATED. THEN THE OVERALL TAILORED PSO ALGORITHM IS MADE AND SUMMARIZED THROUGH A FLOW CHART.

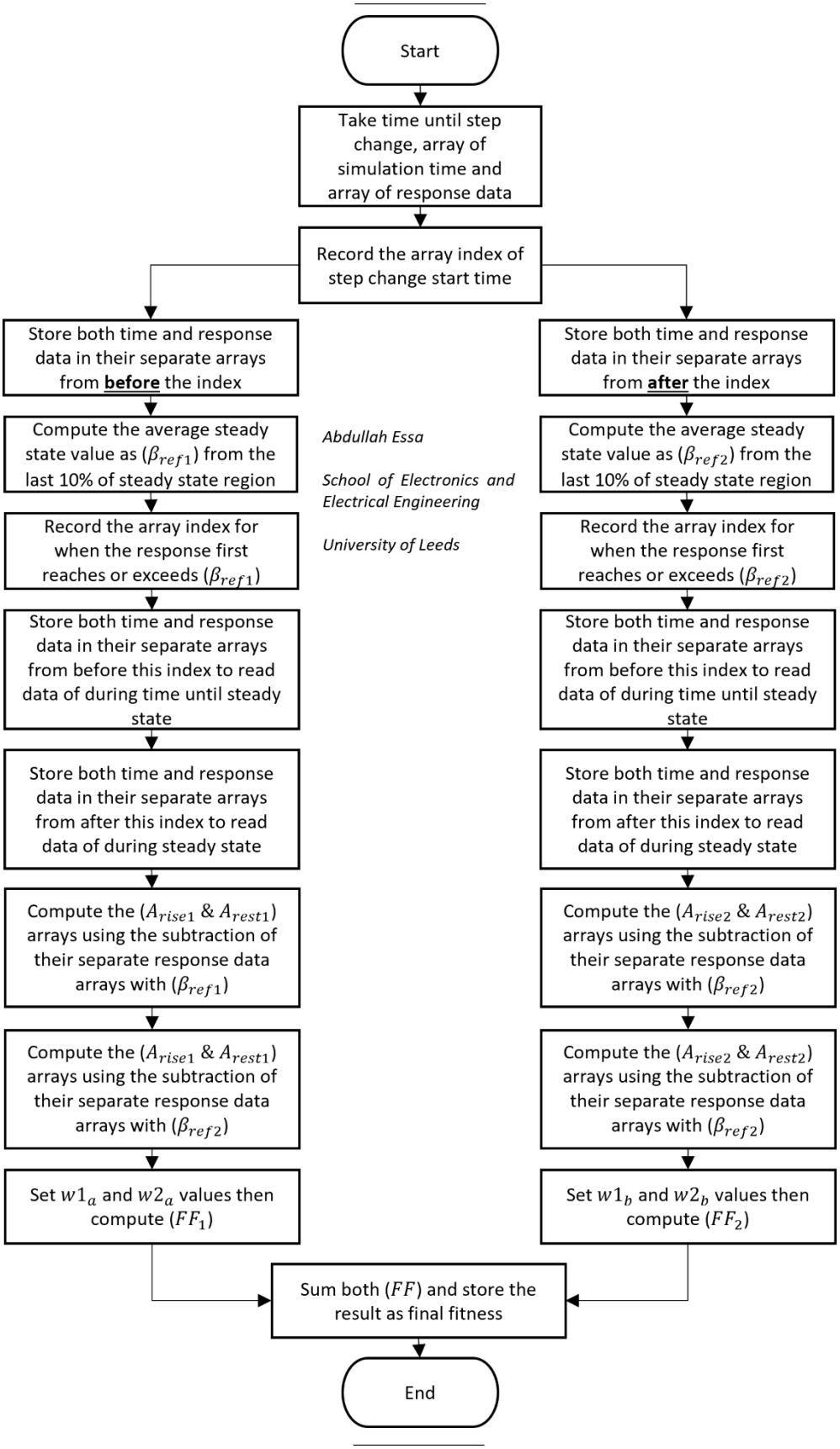

Fig. 17: Fitness Value Attainment Method for The PV Voltage Response and Bus Current Response

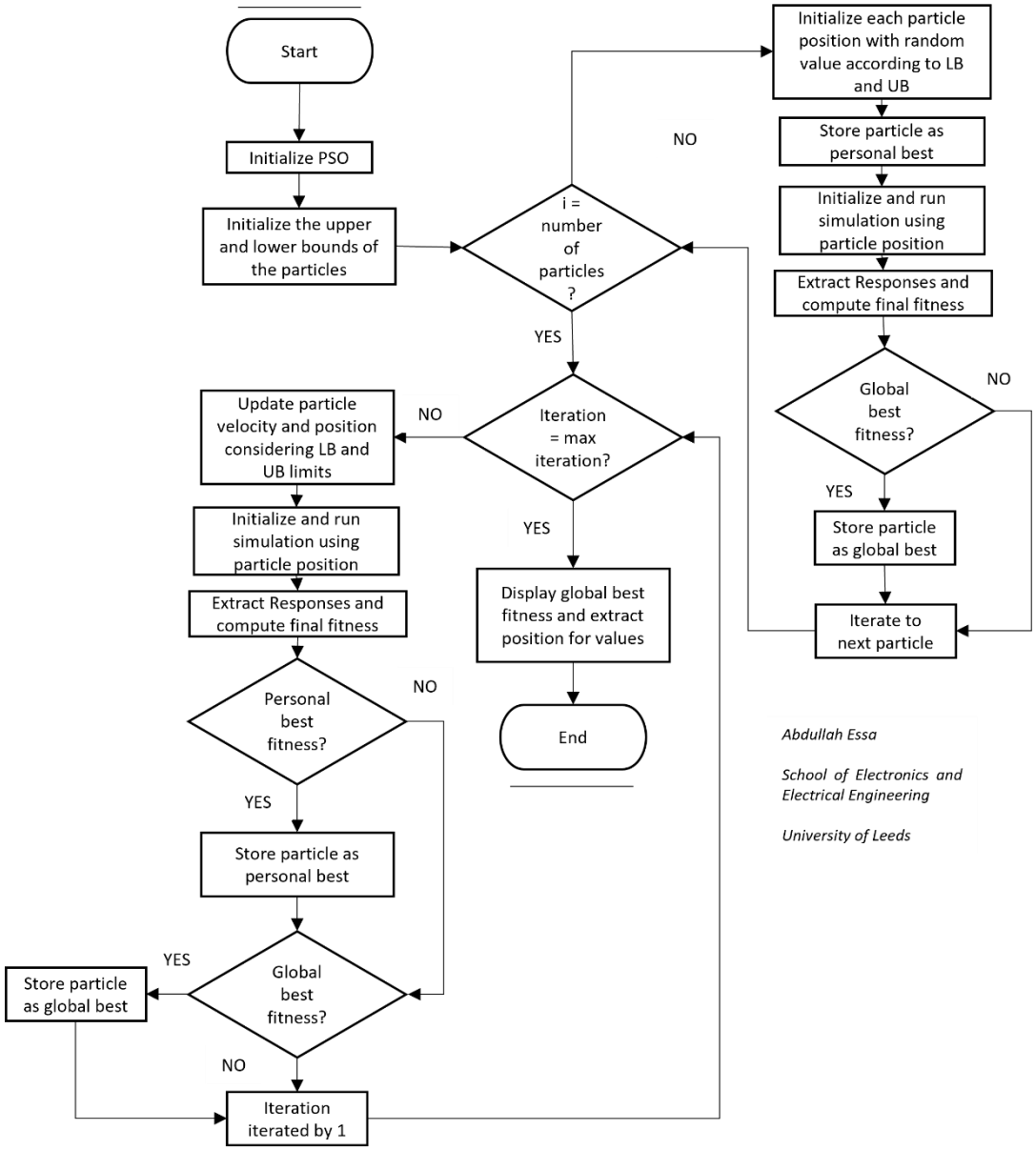

Fig. 18: Overall Tailored PSO Algorithm

IN **Fig. 17**, THE FLOWCHART SHOWS HOW THE FITNESS IS COMPUTED FOR BOTH (V_{PV1} & I_{BUS}). ESSENTIALLY BEFORE THE FUNCTION IS UTILIZED THE SIMULATION WOULD ALREADY HAVE BEEN SIMULATED AND ALL THE RELEVANT DATA FROM THE (**OUT.X**) BLOCK ARE EXTRACTED. CONSEQUENTLY, THEN THE (V_{PV1}, I_{BUS} & SIMULATION TIME) ARE IDENTIFIED TO THEN BE INPUTTED INTO THE FITNESS ATTAINMENT FUNCTION IN **Fig. 17**. THE FITNESS ATTAINMENT FUNCTION THEN DISSECTS THE RESPONSE DATA OF (V_{PV1} & I_{BUS}) AND CREATES A FINAL FITNESS VALUE FOR EACH.

THE FITNESS ATTAINMENT FUNCTION IS THEN UTILIZED IN THE MAIN PSO ALGORITHM SHOWN IN **Fig. 18** THIS A MATLAB SCRIPT THAT INITIALIZES THE PSO ALGORITHM WITH THE NUMBER OF PARTICLES, ITERATIONS, THE UPPER BOUND AND LOWER BOUND VALUES OF THE PASSIVE ELEMENTS (L_1, L_2, C_1, C_2 & C_N). THEN RANDOMLY GENERATES THEIR POSITIONS/VALUES IN ACCORDANCE WITH THE BOUND LIMITS. WHEN CONDITIONS ARE MET TO MOVE ONTO THE NEXT STEP, THE PSO EQUATIONS TO COMPUTE THE NEXT FAVOURABLE POSSIBLE POSITION IS DONE THROUGH **EQUATIONS (18) - (19)**.

HOWEVER DUE TO OPTIMUM RESULT BEING DEPENDENT ON THE SPECIFIC VALUES OF ($\mathbf{C_1}, \mathbf{C_2}$ & $\mathbf{w}$), THEY ARE ASSIGNED A RANDOM VALUE FROM MINIMUM (0.01) TO MAXIMUM (1). THIS CHANGES TO ANOTHER RANDOM VALUE ON EVERY ITERATION SUCH THAT OPTIMUM RESULT IS ACHIEVED STOCHASTICALLY WHICH IS LESS COMPLEX.

B. Optimization Algorithm Analysis

In this section the Simulink model depicted in **Fig. 11** will be optimized via the PSO approach, as outlined in **Fig. 18**.

1. Choice of Upper and Lower Bounds of PSO Inequality Constraints

This optimization process first involves the strategic initialization of upper and lower boundaries for the passive components, namely (L_1, L_2, C_1, C_2 & C_n). This is because when the search space is contained within a smaller space, the optimization finds the solution at a faster pace due to less requirement to increase search particles. Additionally, it is unnecessary to expand the search space into a region where the values are not possible for the application of a PV system DPP converter. This is as very low values end up increasing switching losses and large values end up increasing the package size. Another issue tends to be with the cost and availability of the components. Elaborated in **Appendix (L)** the following upper and lower bounds have been formulated in **Table 6**.

Table 6: Upper and Lower Bound of Passive Components in PV Integrated DPP Cuk Converter

Component	Upper Bound	Lower Bound
L	15 mH	1 mH
C	200 μF	1 μF

2. Choice of (w1) and (w2) in Fitness Attainment

The subsequent analysis aims to investigate the results after changes in (w1 & w2). The weights w1 and w2 are closely associated with two distinct but essential aspects of the system performance, namely, the time to steady-state fitness and the weight of steady-state fitness respectively.

The experimental analysis employs varying sets of values for w1 and w2, aiming to capture the changes and trends in system performance with each modification. The purpose of this investigation is to identify the most favourable combination of these weights, which ultimately enhances the system performance to a reduced time to steady state and/or Rise/Fall Time and steady state ripple.

The varying sets of values for w1 and w2 will be in an increasing order for w1, and w2 will stay constant at 1 as shown in **Table 7**.

Table 7: Variation of w1 and w2 Values

w1	1	5	10	15	20	30
w2	1	1	1	1	1	1

For each distinct pair of w1 and w2 values, five separate simulation runs will be conducted. This approach is necessitated by the inherent stochastic nature of the PSO method when it was developed in **Fig. 18**. Through investigation, the stochastic nature will cause an occasional convergence towards a nearby sub-optimal result (local optimum) instead of the desired optimal result (global optimum). This local convergence is attributed to the method's inability to always navigate through the complex search space to find the global minimum [45], [46]. The fitness before and after optimization for each of the 4 simulations will be recorded and shown through **Tables (8) – (13)**. The simulation run with the minimum fitness after optimization is highlighted in grey.

Table 8: Fitness from Simulation (w1 = 1 & w2 = 1)

Test	Fitness Before	Fitness After
1	1038602.142	899012.1
2	1014113.005	859446.2
3	1049414.396	925856.6058
4	1053686.819	746473.8207
5	1070773.978	776496.9326

Table 9: Fitness from Simulation (w1 = 5 & w2 = 1)

Test	Fitness Before	Fitness After
1	1253952.405	1087444.927
2	1336489.409	1089444.97
3	1539159.555	1120840.144
4	1552739.74	920364.82
5	1570749.071	1093523.731

Table 10: Fitness from Simulation (w1 = 10 & w2 = 1)

Test	Fitness Before	Fitness After
1	1850696.7	1158363.389
2	1688587.076	981554.6196
3	1517520.799	981757.0882
4	1762410.938	1183921.257
5	1717221.912	1155016.6

Table 11: Fitness from Simulation (w1 = 15 & w2 = 1)

Test	Fitness Before	Fitness After
1	2230055.123	1062273.378
2	1696537.762	1173903.525
3	2539525.841	1174548.273
4	2747609.819	1229745.483
5	1659960.45	1061999.57

Table 12: Fitness from Simulation (w1 = 20 & w2 = 1)

Test	Fitness Before	Fitness After
1	3479679.024	1289940.524
2	2290401.072	1136876.83
3	2194498.738	1288696.15
4	2693255.168	1136076.691
5	2033475.989	1295820.177

Table 13: Fitness from Simulation (w1 = 30 & w2 = 1)

Test	Fitness Before	Fitness After
1	5027670.065	1442294.685
2	5178121.348	1436736.148
3	3243748.88	1436569.312
4	4680353.91	1427552.36
5	2177991.661	1288558.604

TO CHECK IF THE PSO METHOD IS WORKING THE SIMULATION WITH MINIMUM FITNESS DEPICTED IN **Table 8** FOR (W1 = 1 & W2 = 1) IS EXAMINED.

THE FIRST ITERATION OF THE PSO ALGORITHM AS SHOWN IN **Fig. 19**, **Fig. 20**, AND **Table 14** DISPLAYS THE OUTCOME OF RANDOM GENERATION OF PARTICLE POSITIONS. THE RANDOM GENERATION GAVE A RESPONSE THAT IS NON-OPTIMAL AS (V_{PV1}) DOES NOT REACH STEADY STATE WITHIN THE GIVEN TIME FRAME.

HOWEVER, THROUGHOUT THE PSO ALGORITHM IN APPENDIX (A) CONSIDERING **16 PARTICLES** AND **22 ITERATIONS**, THE OUTCOME IS IMPROVED. THE RESPONSES ARE SHOWN IN **Fig. 21** AND **Fig. 22** WITH DETAILS IN **Table 15**.

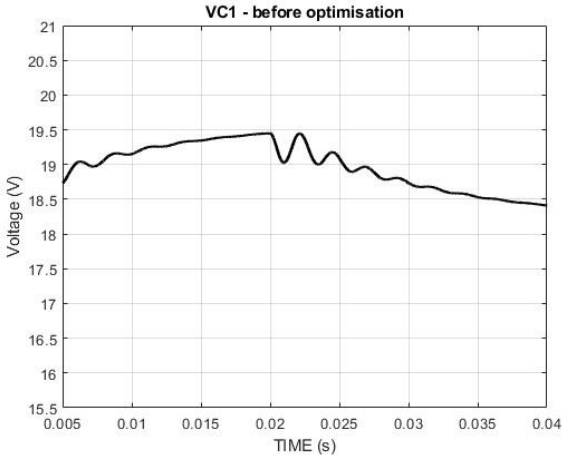

Fig. 19: Analysis of V_{PV1} Response Before Optimization at (w1 = w2 = 1)

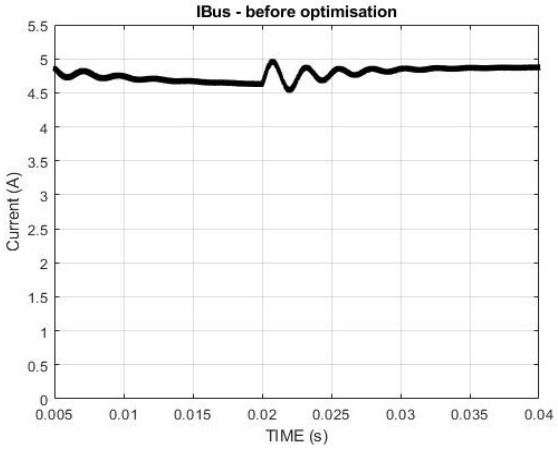

Fig. 20: Analysis of I_{Bus} Response Before Optimization at (w1 = w2 = 1)

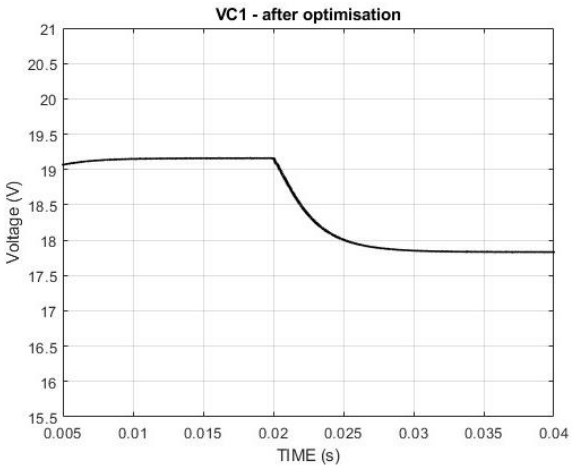

Fig. 21: Analysis of V_{PV1} Response After Optimization at (w1 = w2 = 1)

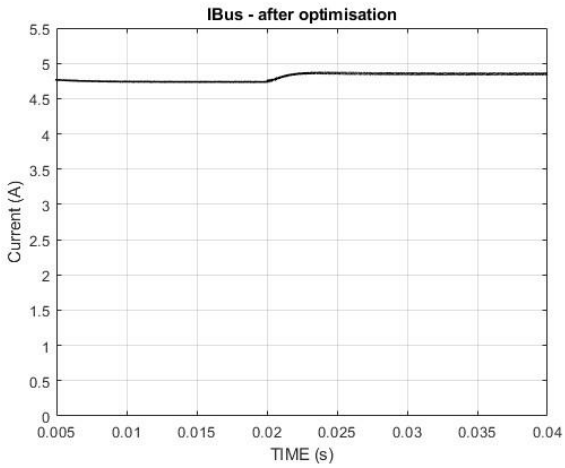

Fig. 22: Analysis of I_{Bus} Response After Optimization at (w1 = w2 = 1)

Table 14: Ripple and Time to Steady State Analysis of Responses Before Optimization at (w1 = w2 = 1)

Before Optimization (w1 = w2 = 1)			
Ripple Vpv (%)	Rise/Fall Time Vpv (s)	Ripple Ibus (%)	Rise/Fall Time Ibus (s)
0.488	[Does not Settle]	1.845	15.1 ms

Table 15: Ripple and Time to Steady State Analysis of Responses After Optimization at (w1 = w2 = 1)

After Optimization (w1 = w2 = 1)			
Ripple Vpv (%)	Rise/Fall Time Vpv (s)	Ripple Ibus (%)	Rise/Fall Time Ibus (s)
0.002	12.3 ms	0.008	2.1 ms

AS DEPICTED IN **Table 15**; THE (V_{PV1}) HAS ITS RIPPLE DECREASED BY FACTOR OF (24.4) FROM 0.488% TO 0.002%, THE RESPONSE NOW SETTLES AS WELL WITHIN 12.3MS. ADDITIONALLY, THE (I_{Bus}) HAS ITS RIPPLE AND TIME TO STEADY STATE BOTH DECREASED FROM 1.845% AND 15.1MS TO 0.008% AND 2.1MS RESPECTIVELY. THIS SHOWS A CLEAR IMPROVEMENT IN PERFORMANCE AS THE PSO ALGORITHM IS INTENDED TO DO.

CONSEQUENTLY, THE RESULTS OF COMPONENT VALUES FOR EACH OF THE MINIMUM FITNESS OUTCOMES FROM TABLES (8) – (13) ARE COMPARED AND SHOWN THROUGH TABLES (16) – (20). THIS IS TO FIND THE OPTIMAL DESIGN THAT WOULD ACHIEVE THE FASTEST RESPONSE WITH MINIMAL RIPPLE.

Table 16: Ripple and Time to Steady State Analysis of Responses After Optimization at (w1 = 5 & w2 = 1)

After Optimization (w1 = 5 & w2 = 1)			
Ripple Vpv (%)	Rise/Fall Time Vpv (s)	Ripple Ibus (%)	Rise/Fall Time Ibus (s)
0.413	3.9 ms	1.522	0.63 ms

Table 17: Ripple and Time to Steady State Analysis of Responses After Optimization at (w1 = 10 & w2 = 1)

After Optimization (w1 = 10 & w2 = 1)			
Ripple Vpv (%)	Rise/Fall Time Vpv (s)	Ripple Ibus (%)	Rise/Fall Time Ibus (s)
0.029	2.4 ms	0.107	1.1 ms

Table 18: Ripple and Time to Steady State Analysis of Responses After Optimization at (w1 = 15 & w2 = 1)

After Optimization (w1 = 15 & w2 = 1)			
Ripple Vpv (%)	Rise/Fall Time Vpv (s)	Ripple Ibus (%)	Rise/Fall Time Ibus (s)
0.02	2.1 ms	0.104	0.62 ms

Table 19: Ripple and Time to Steady State Analysis of Responses After Optimization at (w1 = 20 & w2 = 1)

After Optimization (w1 = 20 & w2 = 1)			
Ripple Vpv (%)	Rise/Fall Time Vpv (s)	Ripple Ibus (%)	Rise/Fall Time Ibus (s)
0.025	1.8 ms	0.091	0.57 ms

Table 20: Ripple and Time to Steady State Analysis of Responses After Optimization at (w1 = 30 & w2 = 1)

After Optimization (w1 = 30 & w2 = 1)			
Ripple Vpv (%)	Rise/Fall Time Vpv (s)	Ripple Ibus (%)	Rise/Fall Time Ibus (s)
0.515	0.82 ms	1.9	0.013 ms

THEIR COMPONENT VALUES ARE SHOWN BELOW IN **Table 21**.

Table 21: DPP Component Values of Each Best Test Case

After Optimization						
Case	**L1**	**L2**	**C1**	**C2**	**Cn**	**Test Number**
(w1 = w2 = 1)	15 mH	0.001 H	12.58 Uf	200 uF	0.5 uF	4
(w1 = 5 & w2 = 1)	5.266 mH	0.001 H	1 Uf	86.63 uF	0.5 uF	4
(w1 = 10 & w2 = 1)	3.2547 mH	0.001 H	27.32 uF	93.067 uF	0.5 uF	2
(w1 = 15 & w2 = 1)	2.7755 mH	0.001 H	20.44 uF	59.42 uF	0.5 uF	5
(w1 = 20 & w2 = 1)	2.445 mH	0.001 H	15.86 uF	40.98 uF	0.5 uF	4
(w1 = 30 & w2 = 1)	2.7232 mH	0.001 H	1 uF	1 uF	0.5 uF	5

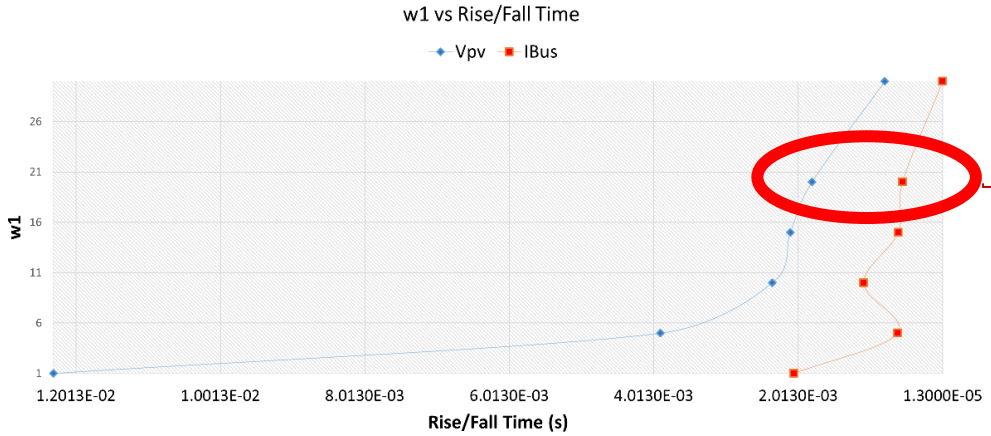

Fig. 23: Rise/Fall time Trend as w1 Increases

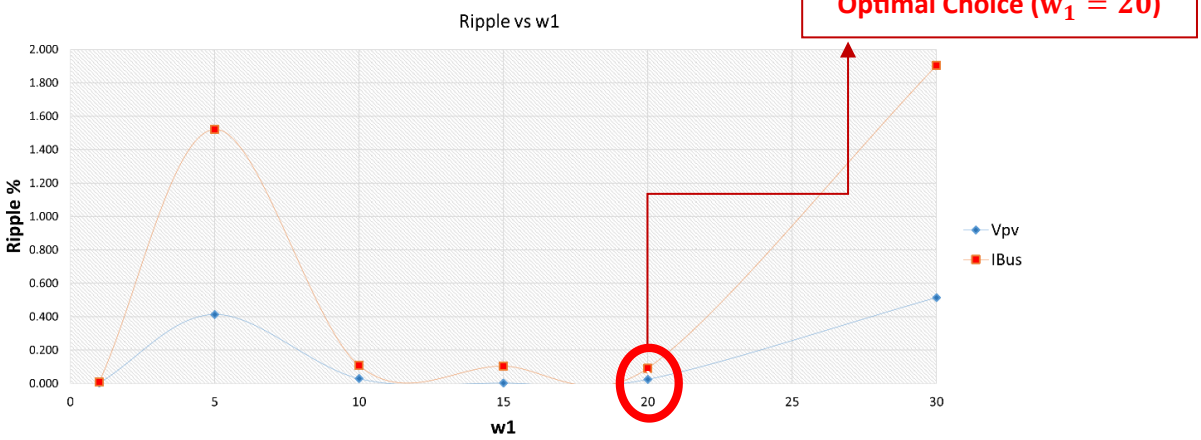

Fig. 24: Rippl e Trend as w1 Increases

HENCE, THE RISE TIME AND RIPPLE TRENDS ARE DEPICTED IN **Fig. 23** AND **Fig. 24** WHICH ARE FORMULATED FROM DATA SHOWN IN TABLES (16) – (20). FROM THE TRENDS, WHEN (W1 =20 & W2 =1), THE PSO ALGORITHM MANAGES TO ACHIEVE THE BEST COMPROMISE BETWEEN RIPPLE AND RISE TIME.

COMPARED TO WHEN (W1 = W2 =1), THE (V_{PV1}) RIPPLE IS OF 0.025% WITH RISE TIME OF 1.8 MS RESPECTIVELY COMPARED TO 0.02% AND 12.3 MS. THE (I_{Bus}) RIPPLE IS OF 0.091% WITH RISE TIME OF 0.57 MS RESPECTIVELY COMPARED TO 0.008% AND 0.63 MS.

THE (V_{PV1} & I_{Bus}) RESPONSES FOR (W1 =20 & W2 =1) ARE SHOWN IN **Fig. 25** AND **Fig. 27**.

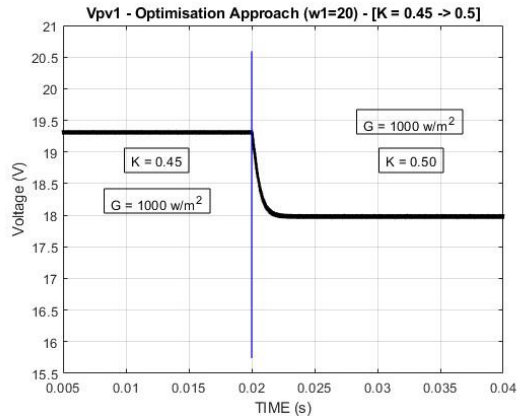

Fig. 25: V_{PV1} Response After Optimization at (w1 = 20 & w2 = 1)

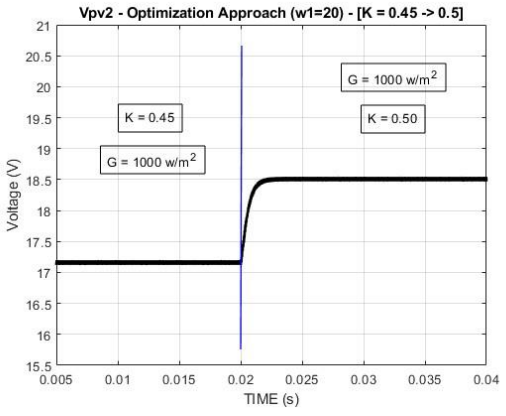

Fig. 26: V_{PV2} Response After Optimization at (w1 = 20 & w2 = 1)

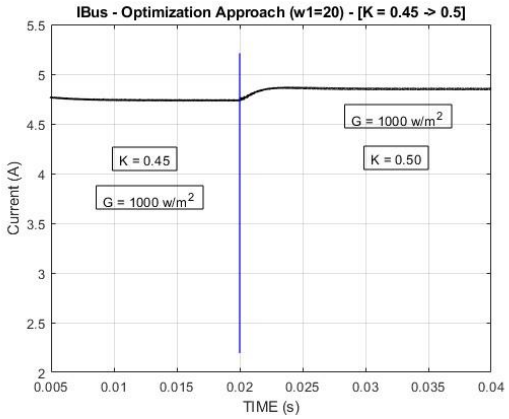

Fig. 27: I_{Bus} Response After Optimization at (w1 = 20 & w2 = 1)

3. Comparison Between Optimal Result and Estimation Equations Approach

In this section the optimal case is compared with the approach that utilizes the estimation **equations (13)-(17)**. This is done via a bar chart built from data in **Table 5** and **Table 19**.

The script used to draw the grouped bar charts is found in **Appendix (G)**.

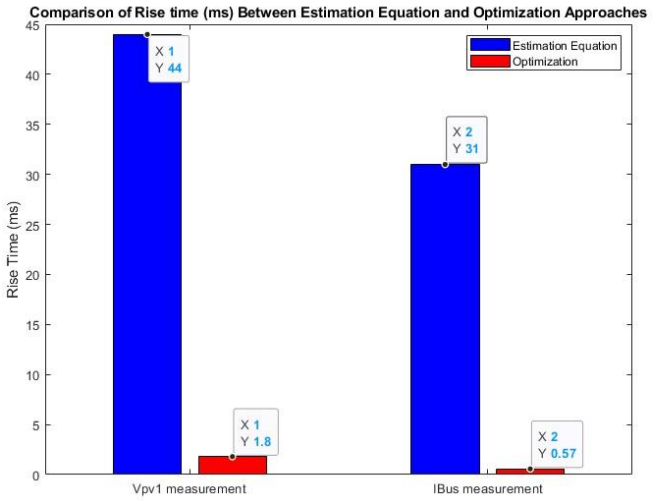

Fig. 28: Bar Chart Comparing Rise Time Between Estimation Equations Approach and Tailored PSO Optimization Approach

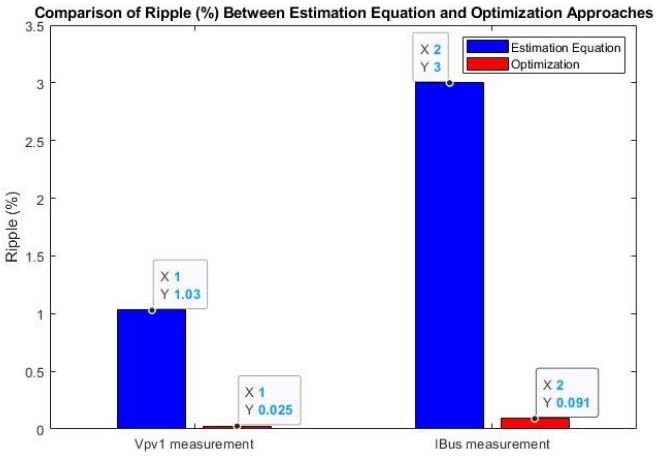

Fig. 29: Bar Chart Comparing Ripple Between Estimation Equations Approach and Tailored PSO Optimization Approach

THE COMPARISON SHOWS CLEAR IMPROVEMENT IN PERFORMANCE WITH THE TAILORED PSO APPROACH COMPARED TO THE ESTIMATION EQUATIONS METHOD. A REDUCTION IN (V_{PV1}) RIPPLE AND RISE TIME BY 1.005% AND 42.2MS RESPECTIVELY. ADDITIONALLY, A REDUCTION IN (I_{BUS}) RIPPLE AND RISE TIME BY 2.909% AND 30.43MS RESPECTIVELY. THE MAIN HANDOUT AND CLEAR IMPROVEMENT ARE WITHIN THE RISE TIME / TIME TO STEADY STATE WHICH IS ACHIEVED WHILST MAINTAINING MINIMAL RIPPLE.

IN THE COMPARATIVE ANALYSIS, (V_{PV2}) HAS NOT BEEN LOOKED AT DUE TO IT EXHIBITING SIMILAR CHARACTERISTICS IN TERMS OF PERFORMANCE TO (V_{PV1}).

IV. CONTROL AND TEST OF PV-PV DPP EMPLOYED VIA INTEGRATED BI-DIRECTIONAL ĆUK CONVERTER ON SIMULINK

IV. Control and Test of PV-PV DPP employed via Integrated Bi-directional Ćuk Converter on Simulink

For this chapter, given the solar irradiance test parameters from the IEC 61853 energy rating standard [48], a model-based control scheme is implemented in this section.

A. Simulink Model Based Track-and-Control

The PV-PV DPP employed via Integrated Bi-directional Ćuk Converter system on Simulink is tested in a manner that PV_2 is undergoing variation in solar irradiance. However, PV_1 is experiencing a constant solar irradiance of $1000\,w/m^2$.

Consequently, the model-based control approach is to have stored quantized values of solar irradiation, each with their corresponding V_{MPP} known beforehand. Thus, through **equation (10)**, the DPP converter switching duty ratio (k) is computed and utilized for maximum power point operation.

---

1. Operation, Approach and Test Parameters

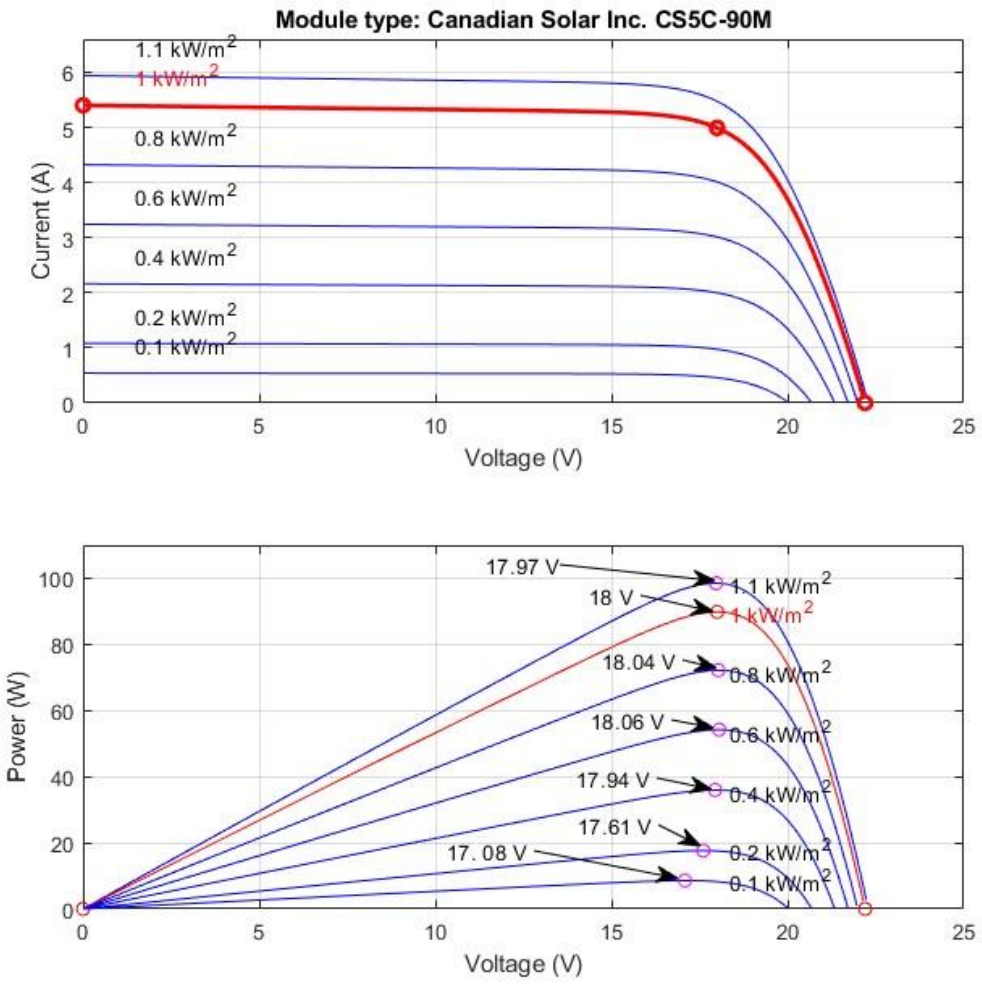

Fig. 30: CS5C-90M Response Characteristics to IEC 61853-1 Irradiance Test Values

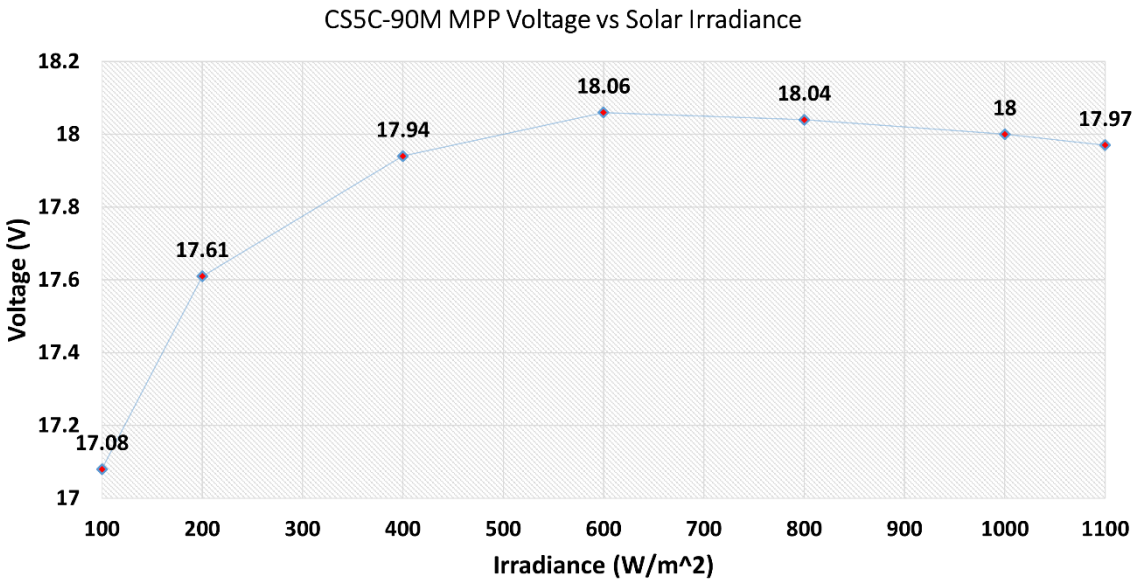

Fig. 31: IEC 61853-1 Irradiance Test Values versus Corresponding V_mpp Value

GIVEN THAT THE IEC 61853 TEST PARAMETERS FOR SOLAR IRRADIATION ARE (1100, 1000, 800, 600, 400, 200, 100) W/M^2 [48] AND TEMPERATURE OF 25°C, THE MODEL WILL BE BASED ON THEIR VALUES. THE DATA POINTS OF SOLAR IRRADIANCE WITH THEIR RELEVANT PV CHARACTERISTICS AND V_{MPP} ARE SHOWN IN **Fig. 30** AND **Fig. 31**.

CONSEQUENTLY, THE (V_{MPP}) TRACK APPROACH IS ELABORATED AS FOLLOWS. IF THE SOLAR IRRADIANCE (G) IS MEASURED TO BE AT $500\ w/m\text{^}2$, THEN WE TAKE THE (V_{MPP}) AT $600\ w/m\text{^}2$ AS (V_{POINT2}) AND TAKE THE (V_{MPP}) AT $400\ w/m\text{^}2$ AS (V_{POINT1}). RESPECTIVELY THEIR IRRADIANCES WILL BE (V_{POINT2}) AND (V_{POINT1}). THOSE VALUES WILL BE USED TO COMPUTE THE GRADIENT (GR) AS SHOWN BELOW.

$$GR = \frac{V_{Point2} - V_{Point1}}{G_{Point2} - G_{Point1}} \qquad (24)$$

THEN, (V_{POINT2}) IS REPLACED WITH (V_{wanted}) SUCH THAT NOW IT REPRESENTS THE (V_{MPP}) OF THE PV PANEL AT THE IRRADIANCE $500\ w/m^2$. **EQUATION (24)** IS THUS REARRANGED SUCH THAT (V_{wanted}) BECOMES THE SUBJECT, AS SHOWN BELOW.

$$V_{wanted} = V_{Point1} - GR(G_{measured} - G_{Point1}) \qquad (25)$$

EQUATION (10) IS THEN REARRANGED SUCH THAT (K_{mpp}) BECOMES THE SUBJECT. THEN (V_{wanted}) IS PLACED IN PLACE OF THE RELEVANT ($V_{PV_{mpp}}$) AS SHOWN BELOW.

$$k_{mpp} = \frac{V_{PV2_{mpp}}}{V_{PV2_{mpp}} + V_{PV1_{mpp}}} \qquad (26)$$

CONSIDERING THE AFOREMENTIONED EQUATIONS, A "MATLAB FUNCTION" BLOCK ON SIMULINK IS UTILIZED TO EXECUTE THE SCRIPT THAT READS THE SOLAR IRRADIATION, THEN COMPUTES THE V_{mpp}. THE BLOCKS RESPONSIBLE FOR/AND OPERATION WITHIN THIS BLOCK IS DEPICTED IN THE NEXT PAGE.

```
function V_mpp = FindVmpp1(G_wanted)

G_wanted1 = G_wanted;
V_wanted1 = 0;
V_point1 = 0;
V_point2 = 0;
G_point1 = 0;
G_point2 = 0;

% IEC 61853 irradiance values
G = [100, 200, 400, 600, 800, 1000, 1100];

% Corresponding mpp voltages
Vmpp = [17.08, 17.61, 17.94, 18.06, 18.04, 18, 17.97];

% deducing mpp voltage
for i = (2:length(G))

    if (G_wanted1 == G(i))
        V_wanted1 = Vmpp(i);
        break;

    elseif (G_wanted1 == G(i-1))
        V_wanted1 = Vmpp(i-1);
        break;

    elseif (G_wanted1 < G(1))

        V_point1 = 0;
        V_point2 = Vmpp(length(Vmpp));
        G_point1 = 0;
        G_point2 = min(G);

        Gradient1 = (V_point2 - V_point1)/(G_point2 - G_point1);
        V_wanted1 = V_point1 + Gradient1*(G_wanted1 - G_point1);
        break;

    elseif (G_wanted1 > G(length(G)))

        V_wanted1 = Vmpp(i);  % cannot find unknown gradient

    elseif (G_wanted1 < G(i) && G_wanted1 > G(i-1))
        % for when the data point is between to known points
        V_point1 = Vmpp(i-1);
        V_point2 = Vmpp(i);
        G_point1 = G(i-1);
        G_point2 =  G(i);

        Gradient1 = (V_point2 - V_point1)/(G_point2 - G_point1);
        V_wanted1 = V_point1 + Gradient1*(G_wanted1 - G_point1);
    end
end

% output result
V_mpp = V_wanted1;
```

Fig. 32: V_{mpp} Look-up Script Inside "Matlab Function" Simulink Block

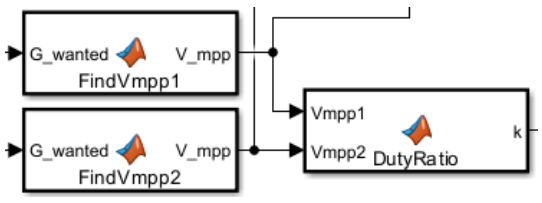

Fig. 33: Connection of V_{mpp} Block to Duty Ratio Compute Block

2. Simulation of Basic Track-and-Control of PV Integrated DPP on Simulink

By using optimal values shown in **Table 21** for the case (w1 =20 & w2 =1), the system is first tested at IEC 61853 irradiance conditions. This is done via a Simulink block named "Signal Builder" creating a step change to the corresponding at IEC 61853 irradiance condition every 0.02 seconds depicted in **Fig. 34**. Then the responses are compared to the equation approach method responses.

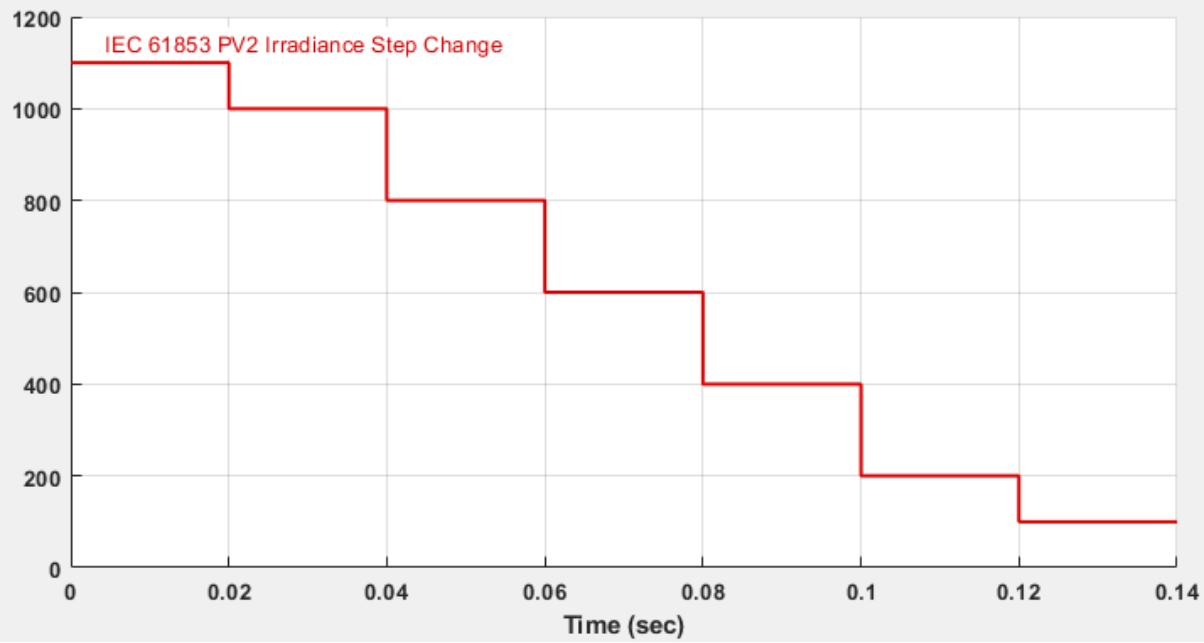

Fig. 34: PV_2 Irradiance Variation on Simulink "Signal Builder" Block

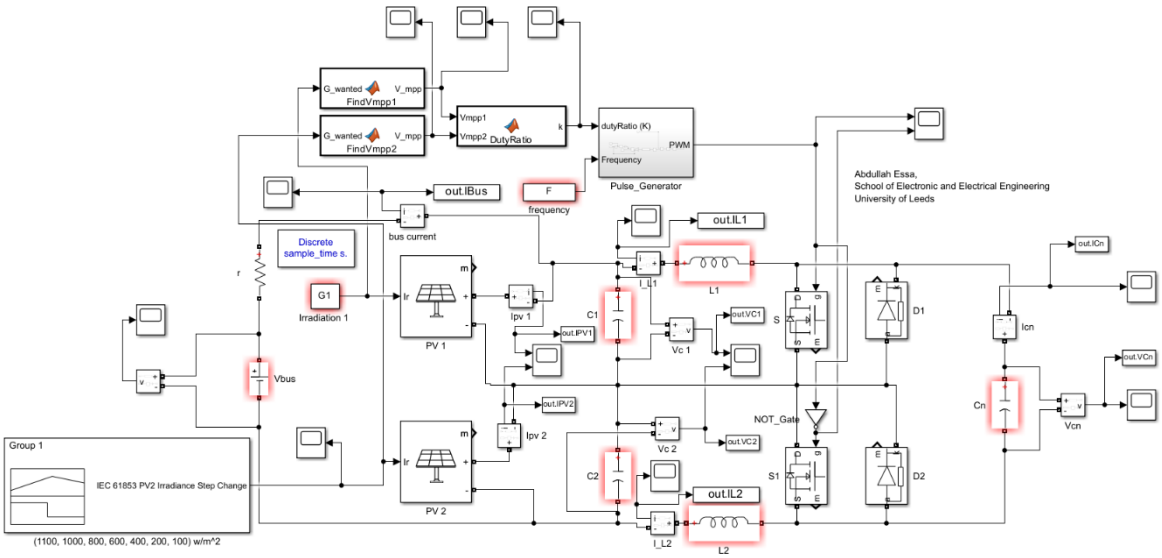

Fig. 35: Track-and-Control PV-PV DPP employed via Integrated Bi-directional Ćuk Converter on Simulink

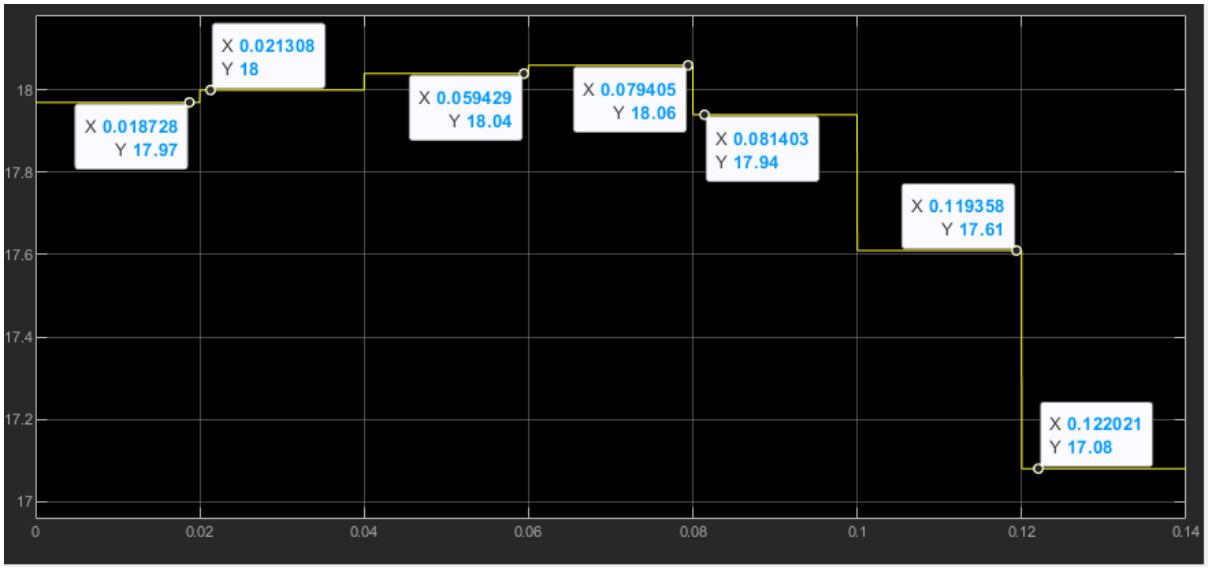

Fig. 36: $V_{PV2_{mpp}}$ Reading from Simulink Scope over Irradiance Variation

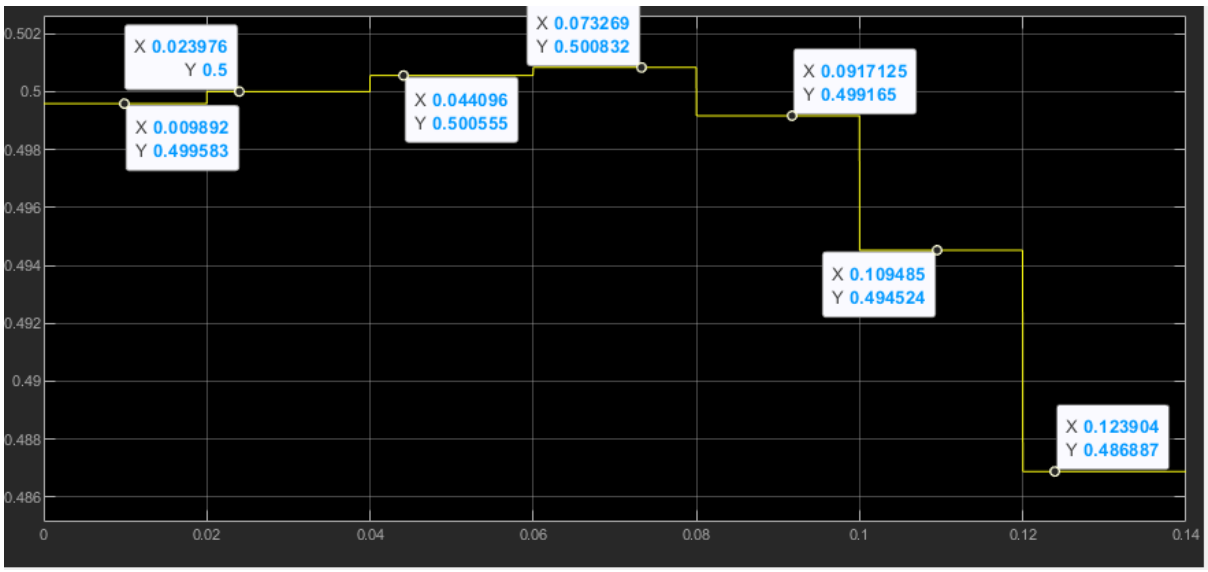

Fig. 37: Duty Ratio Reading from Simulink Scope over Irradiance Variation

Fig. 36 SHOWS (V_{MPP}) FOR EACH IRRADIANCE VALUE EQUAL TO THE (V_{MPP}) VALUES DEPICTED IN **Fig. 31**, WHICH SHOWS THAT THE SCRIPT IS WORKING AS INTENDED.

CONSEQUENTLY, THE COMPUTED DUTY RATIO SHOWS THAT WHEN BOTH PV VOLTAGES ARE EQUAL, WE GET A DUTY RATIO OF ($K = 0.5$) AS MENTIONED IN "INTERIM RESULTS FROM PHASE II – SYSTEM PARAMETERS". WHEN ($V_{PV1} > V_{PV2}$) THEN ($k < 0.5$) AND VICE VERSA.

THE OVERALL PV WITH INTEGRATED DPP SYSTEM IS UPDATED WITH THE AFOREMENTIONED ADDITIONS AND IS SHOWN IN **Fig. 35**.

THE (V_{PV1}, V_{PV2} & I_{BUS}) RESPONSES CORRESPONDING TO THE IEC 61853 IRRADIANCE CONDITIONS ARE SHOWN IN THE NEXT SECTION.

3. SIMULATION COMPARISON, ANALYSIS AND DISCUSSION

THERE IS A CLEAR DIFFERENCE IN THE RIPPLE, OVERSHOOT AND RISE TIMES WHEN COMPARING (V_{PV1}) VIA **Fig. 38** AND **Fig. 41**. MOREOVER, A DIFFERENCE IN THE RISE TIMES WHEN COMPARING (I_{Bus}) VIA **Fig. 40** AND **Fig. 43**. THE OPTIMAL APPROACH HENCE DISPLAYS BETTER PERFORMANCE OVERALL.

HOWEVER, THE OVERSHOOT PHENOMENON IS UNDESIRED AND THE REASON BEHIND ITS OCCURRENCE IS THAT WHEN (PV_2) IS HAS ITS IRRADIANCE STEPPED DOWN AS SHOWN IN **Fig. 39** AND **Fig. 42**, THE CAPACITOR IN PARALLEL DISCHARGES WHICH CAUSES AN UNDERSHOOT SPIKE. KNOWING THAT THE BUS VOLTAGE IS CONSTANT, THE (PV_1) VOLTAGE WILL COUNTERACT THE DECREASE IN (V_{PV2}) AND WILL HAVE ITS OWN SPIKE OVERSHOOT UNTIL THE CAPACITOR CHARGES BACK. ADDITIONALLY, THE (V_{PV1}) SHOULD BE CLOSE TO ITS MPP VOLTAGE DURING ITS CONSTANT $1000\ w/m^2$ IRRADIANCE, HOWEVER THE CHANGE IN (K) DUE TO (PV_2) PARTIAL SHADING IS NUDGING THE OPERATION POINT OF (PV_1) TO A HIGHER VOLTAGE.

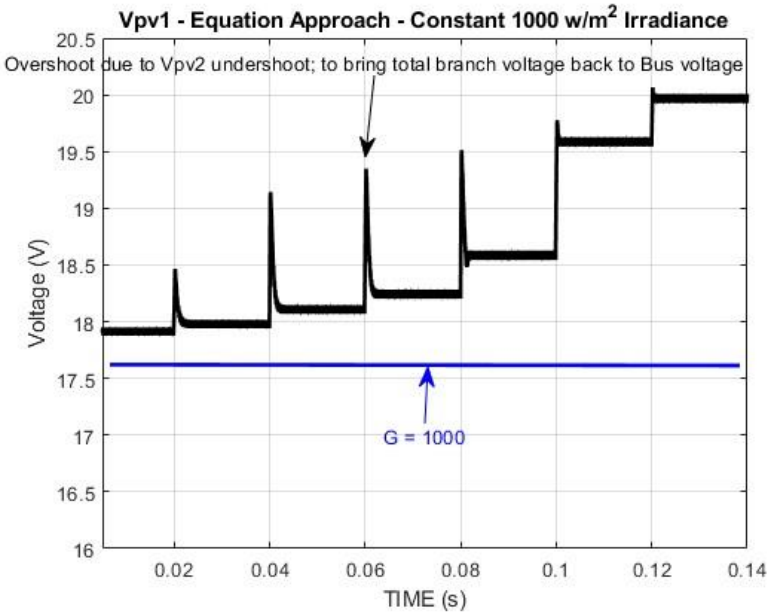

Fig. 38: V_{PV1} Response Over Irradiance Variation Case (w1 =20 & w2 =1)

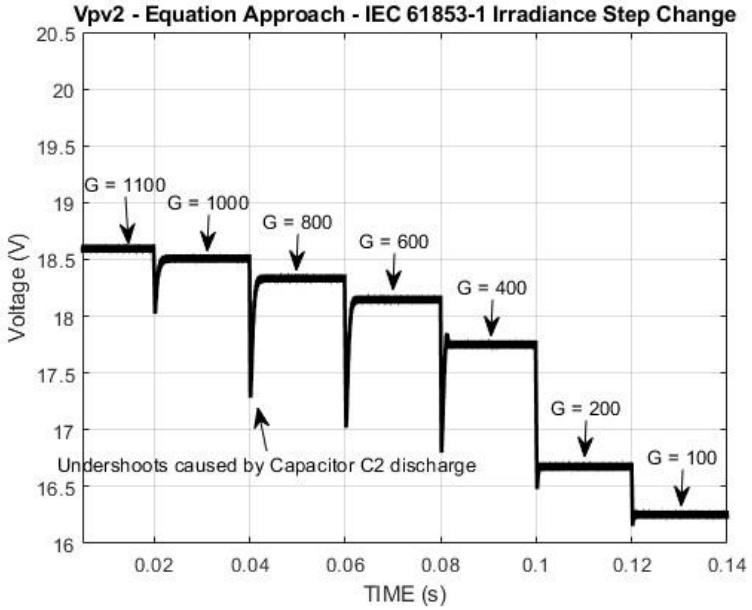

Fig. 39: V_{PV2} Response Over Irradiance Variation Case (w1 =20 & w2 =1)

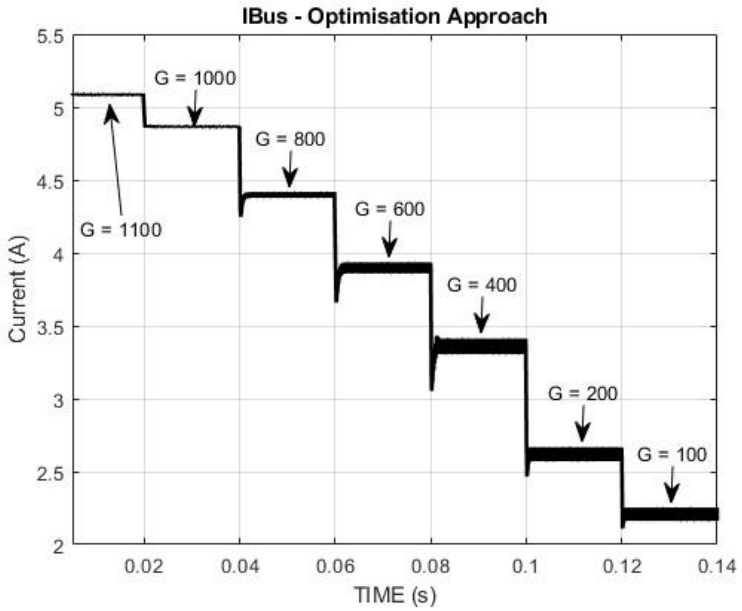

Fig. 40: I_{Bus} Response Over Irradiance Variation Case (w1 =20 & w2 =1)

IN COMPARISON, THE ESTIMATION EQUATIONS APPROACH RESULTS IN THE RESPONSES.

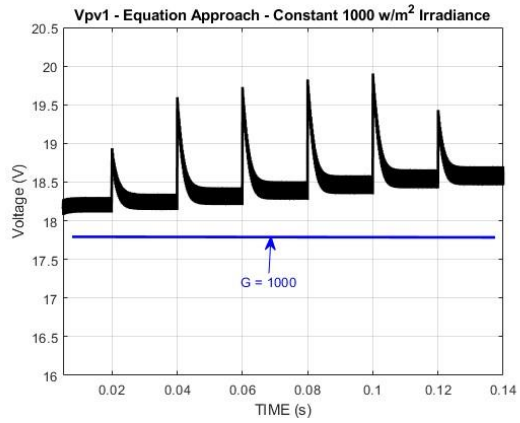

Fig. 41: V_{PV1} Response Over Irradiance Variation Case (Estimation Equations)

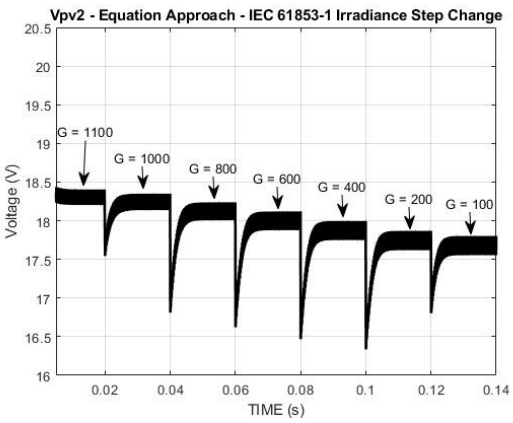

Fig. 42: V_{PV1} Response Over Irradiance Variation Case (Estimation Equations)

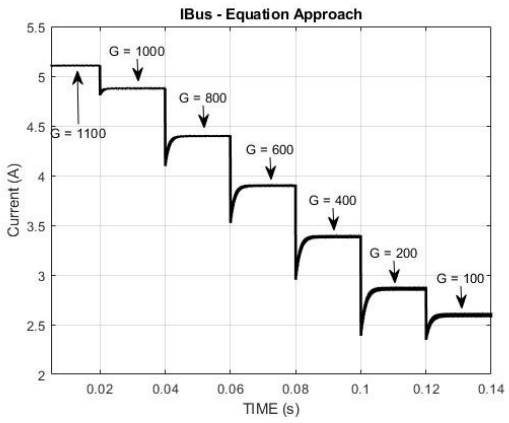

Fig. 43: I_{Bus} Response Over Irradiance Variation Case (Estimation Equations)

V. Conclusion

A. Project Aims and Objectives

This study targets the optimal design and control of DPP converters in PV cells under mismatch conditions, focusing on enhancing power extraction across varied weather scenarios. The main objectives include developing a heuristic optimization method for DPP PV systems using MATLAB and operating an optimally designed Series PV-PV with integrated DPP through a simplified track-and-control method on Simulink.

The optimal design was identified via waveform analysis depicted in **Fig. 15** and **Fig. 16**. After the formulation of the Ćuk DPP converter, five cases were examined, with a rise time weight focus constant of $(w1 = 20)$ yielding the best balance between rise time and ripple. The findings were compared to estimation **equations (13) – (17)** as shown in **Fig. 28** and **Fig. 29**.

Consequently, the PV integrated DPP system was then augmented with "Matlab Function" blocks for simple tracking and control via a look-up table and gradient methodology. Simulations conducted under IEC 61853 irradiance conditions compared the optimal approach to the estimation equations, revealing optimal approach superiority, and MPP control issues, despite achieving the needed duty ratio for MPP operation.

B. SIGNIFICANT TECHNICAL ACHIEVEMENT

THE DEVELOPMENT OF THE FITNESS ATTAINMENT METHOD, ACHIEVED BY EXTRACTING THE RESPONSE WAVEFORM FROM A SIMULINK MODEL AND UTILIZING IT TO ATTAIN AN OPTIMAL RESULT, REPRESENTS THE SALIENT TECHNICAL ACCOMPLISHMENT OF THIS RESEARCH. THIS APPROACH FACILITATED A MORE PROFOUND COMPREHENSION OF THE METHODOLOGY UNDERLYING HEURISTIC OPTIMIZATION, BYPASSING THE COMPLEXITIES ASSOCIATED WITH S-DOMAIN MULTIDIMENSIONAL MATRICES AND TRANSFER-FUNCTION MATHEMATICS. AS THE METHOD IS IMPLEMENTED SOLELY THROUGH THE ANALYSIS OF A WAVEFORM, IT ALLOWS FOR ITS APPLICATION BEYOND THE SCOPE OF THIS STUDY, EXTENDING ITS POTENTIAL USE TO ANY MODELS WHEREIN PERFORMANCE CAN BE ASSESSED THROUGH WAVEFORM ANALYSIS.

C. Future Work

In terms of future work, there's a critical need to upgrade the optimization to handle frequency control to mitigate ripple. Furthermore, handle n number of duty ratio step changes so that the optimal design considers different weather conditions. This can be achieved using the same function used to read the response and determine fitness but executed in a for loop with n iterations at every step time. The fitness of each iteration is added to the next, and the overall total fitness is applied in the PSO algorithm to indicate how far the design is from reaching an optimal state.

Moreover, a more accurate method is necessary for tracking the (V_{MPP}), such as perturb and observe method [33]. This is because the PV characteristic plot isn't always reliable due to changes in temperature and load resistance [33].

Lastly, the PV-integrated DPP will require a DC-DC boost converter connected to a constant supply rather than the constant DC-Bus supply alone. This is because it will be needed to slightly adjust the (V_{BUS}) so that (PV_1) is operating on the (V_{MPP}) considering the DPP switching duty ratio change to adapt to the power flow of the partially shaded (PV_2). A two-level control could be needed, as nudging the partially shaded PV panel to (V_{MPP}) could nudge the other PV panel away from (V_{MPP}) and vice versa with the DC-DC boost converter until an optimal middle ground is found.

D. REFLECTION

OVERALL, THE PROJECT CAN BE CONSIDERED A SUCCESS, ACHIEVING ITS PRIMARY AIM AND OBJECTIVES BY EFFECTIVELY IMPLEMENTING THE HEURISTIC OPTIMIZATION METHOD DEVELOPED SPECIFICALLY FOR DPP PV SYSTEMS. THE SIMULATIONS CONDUCTED PROVIDED VALUABLE INSIGHTS INTO THE SYSTEM'S PERFORMANCE AND CONTROL, ALTHOUGH MINOR ISSUES IN MPP CONTROL DID ARISE, INDICATING ROOM FOR FURTHER REFINEMENT. PARTICULARLY, THE OPTIMIZATION WAS DONE OVER A SINGLE WEATHER CONDITION CHANGE IMPLEMENTED VIA THE STEP CHANGE IN DUTY RATIO (0.45→0.5), SUGGESTING THAT FURTHER MINOR REFINEMENT OF THE OPTIMIZATION ALGORITHM WOULD BE NEEDED IN THE FUTURE. ALONGSIDE THESE TECHNICAL ACHIEVEMENTS, I DEVELOPED SIGNIFICANT SKILLS IN OPTIMIZATION TECHNIQUES, MATLAB PROGRAMMING, AND SYSTEM SIMULATION USING SIMULINK. THE HANDS-ON EXPERIENCE BROADENED MY UNDERSTANDING OF POWER ELECTRONICS, SOLAR PV CELLS, PARTIAL SHADING ISSUES MITIGATION, AND THE BI-DIRECTIONAL OPERATION OF THE ĆUK CONVERTER. FURTHERMORE, THE PROJECT ENHANCED MY SOFT SKILLS, WITH A SPECIAL EMPHASIS ON TIME MANAGEMENT AND ACADEMIC REPORT WRITING. BALANCING VARIOUS PROJECT TASKS WITHIN A TIGHT TIMEFRAME REQUIRED CAREFUL PLANNING, WHILE DRAFTING THE IEEE REPORT DEMANDED PRECISION AND CLEAR ARTICULATION OF COMPLEX CONCEPTS.

APPENDIX

THE FOLLOWING APPENDICES WILL CONTAIN MATLAB R2022B SCRIPTS AND FUNCTIONS FOR THE TAILORED PSO ALGORITHM, RESPONSE ANALYSIS AND FITNESS ATTAINMENT METHOD THROUGH WAVEFORM ANALYSIS. ADDITIONALLY, TWO SIMULINK MODELS ONE FOR A SINGLE STEP CHANGE IN DUTY RATIO AND THE OTHER FOR HANDLING THE IEC 61853 IRRADIANCE CONDITIONS THROUGH BASIC TRACK-AND-CONTROL.

THE GITHUB REPOSITORY CONTAINING ALL THE FILES WILL BE DISPLAYED BELOW:

[https://github.com/el18ae/ELEC5882-MSc-Individual-Project-2022-23.git]

a. TAILORED PSO MAIN MATLAB SCRIPT

File Name
DPP_PSO.m

SCRIPT PREREQUISITE FUNCTIONS: FITNESSRUNVC1.M – FITNESSRUNIBUS.M – FITNESSSUM.M.

SIMULINK MODEL FILE PREREQUISITE: MUT_FINAL.SLX

b. V_{PV1} FITNESS ATTAINMENT THROUGH WAVEFORM ANALYSIS

File Name
FitnessRunVC1.m

SCRIPT PREREQUISITE FUNCTIONS: NONE.

c. I_{Bus} FITNESS ATTAINMENT THROUGH WAVEFORM ANALYSIS

File Name
FitnessRunIBus.m

PREREQUISITE FUNCTIONS: NONE.

d. TOTAL FITNESS ATTAINMENT

File Name
FitnessSum.m

PREREQUISITE FUNCTIONS: FITNESSRUNIBUS.M – FITNESSRUNVC1.M.

e. WAVEFORM RISE TIME AND RIPPLE COMPUTATION

File Name
GetRipple.m

PREREQUISITE FUNCTIONS: NONE.

f. Waveform Response Plot and Analysis

File Name
PlotEvaluateResponse.m

Script prerequisite functions: GetRipple.m.

Simulink model file prerequisite: MUT_final.slx OR MUT_final2.slx

g. Grouped Comparison Bar Chart

File Name
barchart_plotscript.m

Script prerequisite functions: None.

h. Grouped Comparison Bar Chart

File Name
MUT_final.slx

PV Integrated Ćuk DPP Converter [Single Step Change]

i. PV Integrated Ćuk DPP Converter [Track-and-Control]

File Name
MUTfinal2.slx

j. PV Cell Plot Script

File Name
PVCharPlotScript.m

Script prerequisite functions: PVComp.m.

k. PV Cell Modelling, Simulation and Characteristic Plot

File Name
PVComp.m

Prerequisite functions: None.

l. Component Upper and Lower Limit Justification

Inductors utilized in this project are used for the purposes of reducing current ripple. The larger the inductor value, the larger lower the ripple [43] however at the cost at gaining larger packaging sizes [49]–[52]. The same is true with the capacitor values whom of which are focused to reduce and filter the output voltage ripple [43]. Cost is another factor that increases with value increase [49]–[52].

Aiming for a smaller inductor or capacitor value would require an increase in the switching frequency to keep the ripple down [43].

THUS, WHEN LOOKING AT THE CURRENT HANDLING CAPABILITY, AVAILABILITY, AND THE AFOREMENTIONED CHARACTERISTICS THROUGH VENDORS [51], [52]. THE FOLLOWING UPPER AND LOWER BOUNDS HAVE BEEN MADE FOR THE COMPONENTS OF THE DPP.

Component	Upper Bound	Lower Bound
L	$15\ mH$	$1\ mH$
C	$200\ \mu F$	$1\ \mu F$

REFERENCE

[1] H. Jeong, H. Lee, Y.-C. Liu, and K. A. Kim, 'Review of Differential Power Processing Converter Techniques for Photovoltaic Applications', *IEEE Transactions on Energy Conversion*, vol. 34, no. 1, pp. 351–360, Mar. 2019, doi: 10.1109/TEC.2018.2876176.

[2] A. Alenezi and H. A. Hussain, 'A Novel Method for Least Differential Power Processing in PV Systems', in *2022 IEEE Applied Power Electronics Conference and Exposition (APEC)*, IEEE, Mar. 2022, pp. 1070–1077. doi: 10.1109/APEC43599.2022.9773646.

[3] M. T. Gunfaus and H. Waisman, 'Assessing the adequacy of the global response to the Paris Agreement: Toward a full appraisal of climate ambition and action', *Earth System Governance*, vol. 8, p. 100102, Jun. 2021, doi: 10.1016/j.esg.2021.100102.

[4] M. Zgurovsky, M. Kravchenko, K. Boiarynova, K. Kopishynska, and I. Pyshnograiev, 'The Energy Independence of the European Countries: Consequences of the Russia's Military Invasion of Ukraine', in *2022 IEEE 3rd International Conference on System Analysis & Intelligent Computing (SAIC)*, IEEE, Oct. 2022, pp. 1–4. doi: 10.1109/SAIC57818.2022.9923004.

[5] 'European's energy independence impossible unless wind power considered a strategic industry'. https://www.siemensgamesa.com/en-int/newsroom/2022/09/092622-siemens-gamesa-press-release-europe-wind-energy-security-white-paper (accessed Aug. 05, 2023).

[6] 'Russian gas is 50% cheaper for Europe than US LNG — OMV CEO - Business & Economy - TASS'. https://tass.com/economy/1015850 (accessed Aug. 04, 2023).

[7] I. - International Energy Agency, 'Renewable Energy Market Update - June 2023', 2023, Accessed: Aug. 08, 2023. [Online]. Available: www.iea.org/t&c/

[8] Reuters, 'Trump Warns Germany Could Become Reliant On Russian Energy', 2018. https://www.rferl.org/a/trump-warns-germany-could-become-reliant-on-russian-energy/29509218.html (accessed Aug. 04, 2023).

[9] 'Siemens Gamesa strengthens its partnership with European Energy to supply wind farms in Sweden and Poland'. https://www.siemensgamesa.com/newsroom/2020/12/201202-siemens-gamesa-press-release-european-energy-sweden-poland (accessed Aug. 05, 2023).

[10] M. E. Ropp and S. Gonzalez, 'Development of a MATLAB/Simulink Model of a Single-Phase Grid-Connected Photovoltaic System', *IEEE Transactions on Energy Conversion*, vol. 24, no. 1, pp. 195–202, Mar. 2009, doi: 10.1109/TEC.2008.2003206.

[11] M. Etarhouni, B. Chong, and L. Zhang, 'A combined scheme for maximising the output power of a Photovoltaic array under partial shading conditions', *Sustainable Energy Technologies and Assessments*, vol. 50, p. 101878, 2022.

[12] C. M. Amaral da Luz, E. R. Ribeiro, and F. L. Tofoli, 'Differential Power Processing Applied to a Photovoltaic String with Different Modules', in *2021 Brazilian Power Electronics Conference (COBEP)*, IEEE, Nov. 2021, pp. 1–6. doi: 10.1109/COBEP53665.2021.9684040.

[13] K. A. Kim and P. T. Krein, 'Reexamination of Photovoltaic Hot Spotting to Show Inadequacy of the Bypass Diode', *IEEE J Photovolt*, vol. 5, no. 5, pp. 1435–1441, Sep. 2015, doi: 10.1109/JPHOTOV.2015.2444091.

[14] A. M. Ajmal, T. Sudhakar Babu, V. K. Ramachandaramurthy, Dalia. Yousri, and J. B. Ekanayake, 'Static and dynamic reconfiguration approaches for mitigation of partial shading influence in photovoltaic arrays', *Sustainable Energy Technologies and Assessments*, vol. 40, p. 100738, Aug. 2020, doi: 10.1016/j.seta.2020.100738.

[15] M. Kermadi, V. J. Chin, S. Mekhilef, and Z. Salam, 'A fast and accurate generalized analytical approach for PV arrays modeling under partial shading conditions', *Solar Energy*, vol. 208, pp. 753–765, Sep. 2020, doi: 10.1016/j.solener.2020.07.077.

[16] C. G. Lee *et al.*, 'Analysis of electrical and thermal characteristics of PV array under mismatching conditions caused by partial shading and short circuit failure of bypass diodes', *Energy*, vol. 218, p. 119480, Mar. 2021, doi: 10.1016/j.energy.2020.119480.

[17] S. R. Pendem, V. V. Katru, and S. Mikkili, 'Hybrid PV Array Configurations for Reducing the Multiple-Peak Power Points in $I-V$ and $P-V$ characteristics under Partial Shading Conditions', in *TENCON 2019 - 2019 IEEE Region 10 Conference (TENCON)*, IEEE, Oct. 2019, pp. 598–603. doi: 10.1109/TENCON.2019.8929581.

[18] G. Sai Krishna and T. Moger, 'Improved SuDoKu reconfiguration technique for total-cross-tied PV array to enhance maximum power under partial shading conditions', *Renewable and Sustainable Energy Reviews*, vol. 109, pp. 333–348, Jul. 2019, doi: 10.1016/j.rser.2019.04.037.

[19] S. Malathy and R. Ramaprabha, 'Reconfiguration strategies to extract maximum power from photovoltaic array under partially shaded conditions', *Renewable and Sustainable Energy Reviews*, vol. 81, pp. 2922–2934, Jan. 2018, doi: 10.1016/j.rser.2017.06.100.

[20] H. Rezk, A. Fathy, and M. Aly, 'A robust photovoltaic array reconfiguration strategy based on coyote optimization algorithm for enhancing the extracted power under partial shadow condition', *Energy Reports*, vol. 7, pp. 109–124, Nov. 2021, doi: 10.1016/j.egyr.2020.11.035.

[21] Feng Wang, Tianhua Zhu, Fang Zhuo, and Yan Yang, 'Analysis and comparison of FPP and DPP structure based DMPPT PV system', in *2016 IEEE 8th International Power Electronics and Motion Control Conference (IPEMC-ECCE Asia)*, IEEE, May 2016, pp. 207–211. doi: 10.1109/IPEMC.2016.7512286.

[22] M. Uno and K. Honda, 'Panel-to-Substring Differential Power Processing Converter With Embedded Electrical Diagnosis Capability for Photovoltaic Panels Under Partial Shading', *IEEE Trans Power Electron*, vol. 36, no. 9, pp. 10239–10250, Sep. 2021, doi: 10.1109/TPEL.2021.3064706.

[23] A. Mitra, S. Bhowmik, S. Mukherjee, P. Dutta, K. Banerjee, and S. Sarkar, 'Performance Comparison and Design of Passive Components for DC-DC Buck-Boost, Cuk and Sepic Converter', in *2022 IEEE International Conference of Electron Devices Society Kolkata Chapter (EDKCON)*, IEEE, Nov. 2022, pp. 12–17. doi: 10.1109/EDKCON56221.2022.10032936.

[24] C. Jing and Y. J. Bao, 'Characteristics analysis and comparison of buck boost circuit and Cuk circuit', in *2013 5th International Conference on Power Electronics Systems and Applications(PESA)*, IEEE, Dec. 2013, pp. 1–3. doi: 10.1109/PESA.2013.6828219.

[25] A. Mitra, S. Bhowmik, S. Mukherjee, P. Dutta, K. Banerjee, and S. Sarkar, 'Performance Comparison and Design of Passive Components for DC-DC Buck-Boost, Cuk and Sepic Converter', in *2022 IEEE International Conference of Electron Devices Society Kolkata Chapter (EDKCON)*, IEEE, Nov. 2022, pp. 12–17. doi: 10.1109/EDKCON56221.2022.10032936.

[26] R. D. Middlebrook and S. Cuk, 'A general unified approach to modelling switching-converter power stages', in *1976 IEEE Power Electronics Specialists Conference*, IEEE, Jun. 1976, pp. 18–34. doi: 10.1109/PESC.1976.7072895.

[27] D. Pattanaik, R. Dash, and S. C. Swain, 'A Review on Solar Thermal PV Modeling & its Characteristics', in *2018 International Conference on Applied Electromagnetics, Signal Processing and Communication (AESPC)*, IEEE, Oct. 2018, pp. 1–6. doi: 10.1109/AESPC44649.2018.9033370.

[28] F. Jingxun, L. Shaowu, Z. Xianping, and L. Yan, 'Research on Photovoltaic Cell Models: A Review', in *2021 33rd Chinese Control and Decision Conference (CCDC)*, IEEE, May 2021, pp. 1006–1011. doi: 10.1109/CCDC52312.2021.9602658.

[29] A. Essa and S. Al Arefi, 'ELEC5564M Electric Power Generation by Renewable Sources Assignment 2', Leeds, 2023.

[30] G. Walker, 'Evaluating MPPT converter topologies using a Matlab PV Model. Journal of Electrical and Electronics Engineering', *Journal of Electrical and Electronics Engineering*, vol. 21, Jan. 2001.

[31] A. Desai and S. Mikkili, 'Modelling and analysis of PV configurations (alternate TCT-BL, total cross tied, series, series parallel, bridge linked and honey comb) to extract maximum power under partial shading conditions', *CSEE Journal of Power and Energy Systems*, 2020, doi: 10.17775/CSEEJPES.2020.00900.

[32] S. R. Pendem and S. Mikkili, 'Modeling, simulation and performance analysis of solar PV array configurations (Series, Series–Parallel and Honey-Comb) to extract maximum power under Partial Shading Conditions', *Energy Reports*, vol. 4, pp. 274–287, Nov. 2018, doi: 10.1016/j.egyr.2018.03.003.

[33] V. K. Viswambaran, A. Ghani, and E. Zhou, 'Modelling and simulation of maximum power point tracking algorithms & review of MPPT techniques for PV applications', in *2016 5th International Conference on Electronic Devices, Systems and Applications (ICEDSA)*, IEEE, Dec. 2016, pp. 1–4. doi: 10.1109/ICEDSA.2016.7818506.

[34] A. S. K. Chowdhury, K. M. A. Salam, and M. A. Razzak, 'Modeling of MATLAB-Simulink based photovoltaic module using flyback converter', in *2014 9th International Forum on Strategic Technology (IFOST)*, IEEE, Oct. 2014, pp. 378–381. doi: 10.1109/IFOST.2014.6991144.

[35] M. Uoya and H. Koizumi, 'A calculation method of photovoltaic array's operational point for MPPT evaluation based on one variable Newton-Raphson method', in *2012 IEEE Third International Conference on Sustainable Energy Technologies (ICSET)*, IEEE, Sep. 2012, pp. 451–456. doi: 10.1109/ICSET.2012.6357440.

[36] M. Balato and M. Vitelli, 'A new control strategy for the optimization of Distributed MPPT in PV applications', *International Journal of Electrical Power & Energy Systems*, vol. 62, pp. 763–773, Nov. 2014, doi: 10.1016/j.ijepes.2014.05.032.

[37] N. H. Zaini, M. Z. A. Kadir, M. Izadi, N. I. Ahmad, M. A. M. Radzi, and N. Azis, 'The effect of temperature on a mono-crystalline solar PV panel', in *2015 IEEE Conference on Energy Conversion (CENCON)*, IEEE, Oct. 2015, pp. 249–253. doi: 10.1109/CENCON.2015.7409548.

[38] S. Chinyoka, T. Ncube, M. Iroegbu, and S. M. S. Alarefi, 'Partial Shading Performance Evaluation of Bifacial PV Array Configurations', in *2020 IEEE International Women in Engineering (WIE) Conference on Electrical and Computer Engineering (WIECON-ECE)*, IEEE, Dec. 2020, pp. 485–488. doi: 10.1109/WIECON-ECE52138.2020.9397975.

[39] R. Ramabadran and D. Mathur, 'Impact of partial shading on solar PV module containing series connected cells', *SHORT PAPER International Journal of Recent Trends in Engineering*, vol. 2, Dec. 2009.

[40] J. W. Bishop, 'Computer simulation of the effects of electrical mismatches in photovoltaic cell interconnection circuits', *Solar Cells*, vol. 25, no. 1, pp. 73–89, Oct. 1988, doi: 10.1016/0379-6787(88)90059-2.

[41] M. Etarhouni, 'Module Integrated DC-DC converters for Photovoltaic (PV) panel', University of Leeds, 2015.

[42] L. Zhang, A. Dehghani, and B. Chong, 'Optimal design of Cuk step-up converter for photovoltaic energy systems', in *5th IET International Conference on Power Electronics, Machines and Drives (PEMD 2010)*, Institution of Engineering and Technology, 2010, pp. 225–225. doi: 10.1049/cp.2010.0186.

[43] N. Mohan, T. M. Undeland, and W. P. Robbins, *Power Electronics. Converters, Applications and Design*, 3rd ed. ohn Wiley and Sons, Inc, 2003.

[44] R. C. Chen, *Designing Low-Ripple DC-DC Converters*. CRC Press, 2012.

[45] J. (n. d.) Zhu, *Optimization of Power System Operation*. Wiley-IEEE Press, 2008.

[46] M. Basu, 'Particle Swarm Optimization Based Goal-Attainment Method for Dynamic Economic Emission Dispatch', *Electric Power Components and Systems*, vol. 34, no. 9, pp. 1015–1025, Sep. 2006, doi: 10.1080/15325000600596759.

[47] A. Essa, 'Dynamic Economic and Environmental Dispatch Considering Plug-in Electric Vehicles', Individual Project, University of Leeds, Leeds, 2021.

[48] A. Driesse and J. Stein, 'From IEC 61853 power measurements to PV system simulations.', Albuquerque, NM, and Livermore, CA (United States), Apr. 2020. doi: 10.2172/1615179.

[49] 'HOME | Murata Manufacturing Co., Ltd.' https://www.murata.com/ (accessed Aug. 10, 2023).

[50] 'TDK Corporation | TDK'. https://www.tdk.com/en/index.html (accessed Aug. 10, 2023).

[51] ‘DigiKey United Kingdom - Electronic Components Distributor’. https://www.digikey.co.uk/ (accessed Aug. 10, 2023).
[51] ‘element14 Community - element14 Community’. https://community.element14.com/#pifragment-12485=6 (accessed Aug. 10, 2023).